Article

Excitation-Wavelength Dependent Photocycle Initiation Dynamics Resolve Heterogeneity in the Photoactive Yellow Protein from Halorhodospira halophila

Masato Kumauchi, L. Tyler Mix, Elizabeth C. Carroll, Dmitry Morozov, Jie Pan, Wendy R. Gordon, Andrew Philip, Jack Fuzell, Ivo H.M. van Stokkum, Gerrit Groenhoff, Wouter D. Hoff, and Delmar S. Larsen

Biochemistry, **Just Accepted Manuscript** • DOI: 10.1021/acs.biochem.7b01114 • Publication Date (Web): 21 Feb 2018

Excitation-Wavelength Dependent Photocycle Initiation Dynamics Resolve Heterogeneity in the Photoactive Yellow Protein from *Halorhodospira halophila*

L. Tyler Mix[†], Elizabeth C. Carroll[†a], Dmitry Morozov [ϕ], Jie Pan[†b], Wendy Ryan Gordon[#c], Andrew Philip[⊥d], Jack Fuzell[†], Masato Kumauchi[§e], Ivo van Stokkum[‡], Gerrit Groenhof [ϕ] Wouter D. Hoff*[§], and Delmar S. Larsen*[†]

[†]*Department of Chemistry, University of California, Davis*
One Shields Avenue, Davis, California 95616

[‡]*Faculty of Sciences, Vrije Universiteit Amsterdam,*
De Boelelaan 1081, 1081 HV Amsterdam, The Netherlands

[§]*Department of Microbiology and Molecular Genetics*
Oklahoma State University, Stillwater, Oklahoma 74078

[#]*Department of Chemistry and* [⊥]*Department of Biochemistry and Molecular Biology*
University of Chicago, Chicago, Il 60637

[ϕ]*Department of Chemistry and NanoScience Center,*
University of Jyväskylä, 40014, Jyväskylä, Finland

[a]Current address: Department of Imaging Physics, Delft University of Technology, Lorentzweg 1, 2628 CJ Delft, the Netherlands

[b]Current address: Department of Physics, Florida International University, Modesto A. Maidique Campus, 11200 SW 8th Street, ECS 450, Miami, FL 33199

[c]Current address: Department of Biochemistry, Molecular Biology and Biophysics, The University of Minnesota, Twin Cities, 6-155 Jackson Hall, 321 Church Street SE, Minneapolis, MN 55455

[d]Current address: Genesis Health System, 1227 E. Rusholme Street, Davenport, IA 52803

[e]Current address: Science Department, Sanshinkinzoku, Co. Ltd, 2-5-20 Niihama, Tadaoka-cho, Senboku-gun, Osaka 595-0814, Japan

Corresponding authors: dlarsen@ucdavis.edu and wouter.hoff@okstate.edu

FUNDING

This work was supported by a grant from the National Science Foundation (CHE-1413739) to both D.S.L. and W.D.H. Additionally, W.D.H. acknowledges additional support from NSF grants MCB-1051590 and MRI-1338097. G.G. and D.M. acknowledge support from the Academy of Finland (grants 258806, 290677, 304455 to G.G. and grant 285481 to D.M.). We also wish to acknowledge CSC - IT Center of Science, Finland, for computational resources.

DEFINITIONS

Abbreviations used in this paper: PYP – Photoactive Yellow Protein, Hhal – *Halorhodospira halophila*, WT – Wild Type, *p*CA – *para*-Coumaric Acid, PAS – Per-Arnt-Sim, BLUF – Blue Light Using FAD. FAD – Flavin Adenine Dinucleotide, LOV – Light-Oxygen-Voltage, FWHM – Full Width at Half Maximum, NOPA – Nonlinear Optical Parametric Amplifier, TA – Transient Absorption, GROMACS - Groningen MAchine for Chemical Simulation, TIP3P- Transferable Intermolecular Potential with 3 Points, NPT – constant N, constant Pressure and constant Temperature, GAMESS(US) - General Atomic and Molecular Electronic Structure System US variant, VEE – Vertical Excitation Energies, XMCQDPT2 - eXtended Multi-Monfigurational Quasi-Degenerated Perturbation Theory, CASSCF - Complete Active Space Self-Consistent Field S/N – Signal to Noise Ratio, PP – Pump-Probe, QM/MM – Quantum Mechanics/Molecular Mechanics, GSB – Ground State Bleach, ESA – Excited State Absorptions, SE – Stimulated Emission, GSI – Ground State Intermediate, EADS – Evolution Associated Difference Spectrum, SADS – Species Associated Difference Spectrum

Abstract

Photoactive Yellow Proteins (PYP) are a diverse class of blue-light absorbing bacterial photoreceptors. Electronically excitation of the p-coumaric acid chromophore covalently bound within PYP results in tri-phasic quenching kinetics, however, the molecular basis of this behavior remains unresolved. Here we explore this question by examining and the excitation wavelength dependence of the photodynamics of the PYP from *Halorhodospira halophila* via a combined experimental and experimental approach. The fluorescence quantum yield, steady state fluorescence emission maximum and cryotrapping spectra are demonstrated to depend on excitation wavelength. We also compare the femtosecond photodynamics in PYP upon two excitation wavelengths (435 nm and 475 nm) with a dual-excitation-wavelength-interleaved pump-probe (DEWI-PP) technique. Multicompartment global analysis of these data demonstrates that the excited-state photochemistry of PYP depends subtly, but convincingly, on excitation wavelength with a similar kinetics, but distinctly different spectral features including a shifted ground-state beach, altered stimulation emission oscillator strengths and peak positions. Three models involving either multi-excited-states, vibrational enhance barrier crossing and inhomogeneity are proposed to interpret the observed excitation wavelength dependence of the data. Conformational heterogeneity was identified as the most probably model, which model was supported with molecular mechanics simulations that identifies two levels of inhomogeneity involving the orientation of the R52 residue and different hydrogen bonding networks to the p-coumaric acid chromophore. Quantum calculations were used to confirm that these inhomogeneities track to altered spectral properties consistent with the experimental results.

Introduction

The Photoactive Yellow Protein (PYP) family of photoreceptors are small single-domain proteins sensitive to blue-light excitation. While over 140 members of this family have been identified in known genomes, only a few have been expressed and characterized.[1, 2] The most studied representative of this family is the PYP from *Halorhodopspira halophila* (Hhal PYP). Hhal PYP is a 125-residue water-soluble Per-Arnt-Sim (PAS) domain containing a thiol-ester linked *para*-coumaric acid chromophore[3] (4-hydroxycinnamic acid, or *p*CA) that gives PYP its characteristic yellow color (Figure 1). PYP naturally controls phototaxis in the purple bacteria *H. halophila*[4] and the production of biofilms in the bacteria *Idiomarina ioihiensis*.[5]

Recently, PAS containing photoreceptors such as BLUF domains (sensors of blue-light using FAD), LOV (Light-oxygen-voltage-sensing) domains, and PYPs[6, 7] have become key targets for engineering novel optogenetics materials because they bind a variety of chromophores and enable sensory activities.[8, 9] Optogenetic materials provided researchers optical control over biological processes by engineering foreign photoreceptors to activate or deactivate cellular functions. Examples of optogenetics include photo-control of ionic currents, messenger molecules, and gene expression.[8, 9] Photoreceptors like PYP can be linked *in vivo* to enzyme domains to create novel light-activated switches for regulating processes in biological systems.[7]

The *in vitro* photoactivity of PYP from *H. halophila* has been studied extensively since its discovery in 1987 by Meyer et al.[10] The photochemistry of PYP involves an excited-state *trans-cis* photoisomerization of *p*CA around the double bond that rapidly quenches fluorescence within several picoseconds, and triggers a reversible photocycle (Figure 1).[11, 12] Photoisomerization of *p*CA results in a temporary intermediate with a red-shifted absorption spectrum, named I_0, after tens of picoseconds.[13] The spectrum of I_0 then blue-shifts and narrows with the formation a

second intermediate, called pR, within a few nanoseconds.[14] After 250 microseconds, the pR state is protonated to form the pB state that initiates a large scale unfolding of the protein backbone.[15, 16] The protonated signaling state with altered protein geometry thermally relaxes to the starting pG state within a second[17] and is ready to begin the cycle again.

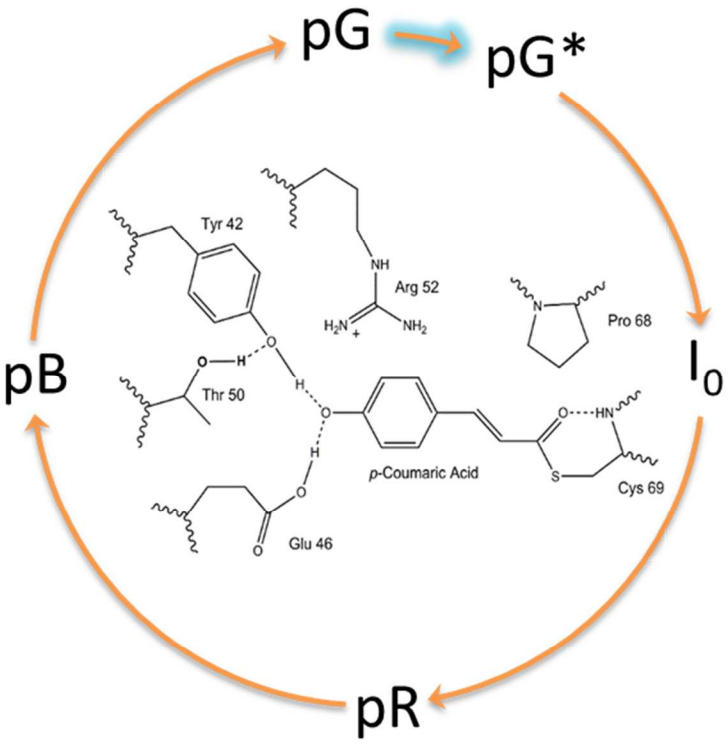

Figure 1: Simple PYP photocycle model with protein pocket of Hhal PYP surrounding the *p*-Coumaric Acid chromophore.

Three decades of studies on the blue-light photoactivity of PYP has resulted in rich information on PYP photochemistry with over 40 different published transient studies on WT Hhal PYP (Table S1).[13, 18-60] These studies have used a broad range of excitation wavelengths (Figure 2) that span the entire pG absorbance spectra (black curve) with 400 nm as the most common excitation wavelength, due to its ease of generation from modern Ti:Sapphire lasers.

The multitude of studies at differing excitation wavelengths present a confusing picture of PYP dynamics with no agreement on the appropriate model.

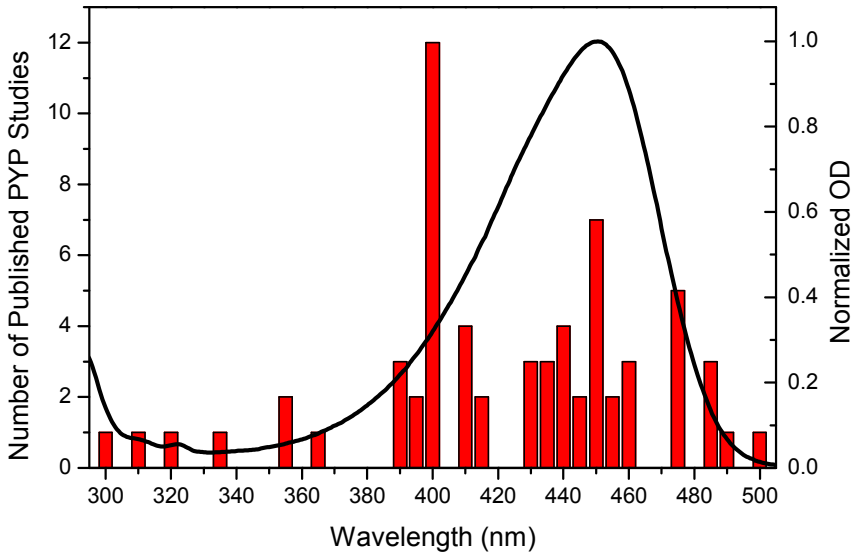

Figure 2: HhaI PYP WT pG absorbance spectrum (black) overlaid with the histogram of the number of photodynamics studies performed with a given excitation wavelength. Includes ultrafast transient absorbance, ultrafast fluorescence, low temperature and crystallographic techniques (Table S1).[13, 18-60]

From cryogenic trapping measurements, Imamoto et al. proposed a branched model that entails two pathways that separate early in the photocycle before recombining to evolve sequentially.[20] A similar heterogeneous branching model was proposed by for ultrafast room-temperature dynamics from PP experiments[28] and by Mix et al.[59] from cryokinetics measurements. The observed ultrafast primary (100 fs-10 ns) photodynamics are often multi-exponential, although researchers disagree on the timescales, amplitudes and even number of exponentials. For example, mid-IR pump – probe (PP) study by Groot and co-workers identified two excited-state lifetimes for HhaI PYP photodynamics: 2 ps and 9 ps,[32] while visible PP measurements identified three excited state lifetimes: 500-fs, 2-ps and 40-ps,[24, 35, 59] despite both techniques resolving the same excited-state quenching dynamics. Some groups argued for a homogeneous-

unidirectional-branching model from time-resolved crystallography measurements,[46, 52, 61] although an alternative transient crystallography study by Anfinrud and coworkers proposed a homogeneous-bidirectional-sequential model for pR production.[51] A homogeneous-unidirectional-sequential model was proposed for room temperature evolution by Cusanovich and coworkers.[24, 62] Even within sequential models, disagreements exist: a second intermediate photoproduct state, $I_0^{\ddagger}$, has been proposed between the I_0 and pR photocycle states,[13] that is not confirmed in other PP studies. No model has been firmly established, which may be due in part to the wide range of excitation wavelengths between experiments (Figure 2).

Despite several studies addressing the wavelength dependence of Hhal PYP photochemistry, no consensus has been reached so far on the interpretation of this dependence, nor on its biological significance, if any. Imamoto argued from low temperature absorption and fluorescence signals that the yield of photochemical intermediates of PYP is excitation-wavelength dependent.[20] It is unclear how the cryogenically frozen Hhal PYP dynamics extend to the primary dynamics of PYP under physiological temperatures. Devanathan et al. proposed a different pathway for formation of I_0 initiated by 395 nm versus 460 nm excitation pulses, but did not extend their study into the ns regime required to characterize pR formation dynamics.[24] An ultrafast anisotropy experiment by Gensch et al. first observed that photoisomerization occurs in the I_0 state with 400-nm and 485-nm excitation beams, but did not observe pR formation dynamics.[30] Both studies clearly demonstrated that excitation wavelengths on the low and high energy sides of PYP's absorption band initiate different photodynamics (Figure 2; black curve).[24, 30] Unfortunately, the data reported by both groups were compromised by solvated electrons created from 2-photon absorption of high energy ultrafast pulses prompting *p*CA ionization.[35] This process is an artifact of the high intensity ultrafast excitation conditions and

presumably has no significant influence on the photoresponse of PYP under ambient light conditions, but complicates the resulting analysis with excitation wavelengths < 430 nm. Carroll et al.[48] demonstrated that PYP responds to UV light due to Förster resonance energy transfer (FRET) interactions with nearby Trp119, but did not investigate the wavelength dependence beyond characterizing the new initiation pathway.

Due to the limitations in published work on Hhal PYP wavelength dependence, the field would benefit from a more sensitive experimental approach to reliably quantify excitation wavelength dependences of PYP photochemistry that could be applied *in vivo*. Here we report a comprehensive excitation wavelength dependence study of Hhal PYP WT using the primary excited state femtosecond dynamics, the steady state fluorescence, cryotrapped spectra and quamtum-mechanics/molecular mechanics (QM/MM/0 simulations to reveal and quantify excitation wavelength dependence in the photocycle. We use an experimental method based on a dual excitation wavelength interleaved pump-probe (DEWI-PP) approach[63, 64, 65] whereby two alternating broadband pump-probe signals are collected near simultaneously (within 4 ms), while all other experimental conditions are essentially unchanged. The DEWI-PP approach has been successfully used to resolve wavelength dependent dynamics of cyanobacteriochromes NpR6012g4,[65] RcaE[64] and β-carotene.[63] DEWI-PP removes errors caused by long-term fluctuations of excitation power, sample degradation, and different experimental conditions and constitutes a powerful approach for identifying small, but significant and potentially informative excitation-wavelength dependence of transient absorption signals.[66] Three distinct explanations for the observed wavelength dependency are considered: multiple electronic excited states, vibrationally enhanced dynamics, or heterogenous ground and excited states.

Experimental Methods

Sample preparation. N-terminal Histidine-tagged wild type *apo*PYP from *H. halophila* was over expressed in *E.coli* (BL21 DE3) and extracted with 8 M urea as described.[67, 68] The *apo*PYP was diluted two-fold using a 10 mM Tris-HCl buffer at pH 7.5 and was reconstituted by the addition of an excess of *p*-coumaric acid anhydride (Sigma Aldrich). After removal of the urea by dialysis against 10 mM Tris-HCl buffer at pH 7.5, the protein was purified by chromatography on a Ni-NTA resin (using 200 mM imidazol as the eluent) and DEAE-sepharose CL6B (using 100 mM NaCl for elution) until a purity index (defined as the ratio of the absorption of 446 nm to 278 nm) of less than 0.45 was achieved.

Fluorescence spectroscopy. Fluorescence excitation and emission spectra were measured in a SPEX Fluoromax-3 fluorimeter (Jobin-Yvon) using a cuvette with a 100 μL nominal volume (Starna #16.100F-Q-10/Z15; ~130 μL is needed to avoid scattering from the meniscus). Since the shape of the fluorescence emission spectra of Hhal PYP is independent of excitation wavelength (see Figure 3A; blue and red curves), the amplitude of the emission peak was used to estimate the wavelength dependence of fluorescence quantum yield. This is equivalent to dividing the excitation spectrum of PYP by its absorbance spectrum. We used two approaches to confirm that inner filter effects did not perturb the observed excitation wavelength dependence of fluorescence quantum yield: (1) the sample concentration was adjusted to obtain an absorbance of less than 0.1 at the excitation wavelength and (2) the fluorescence emission spectra were measured for samples with different PYP concentrations to ensure a linear relationship between emission intensity and sample absorbance.

Cryotrapping Spectroscopy. The low temperature cryotrapping measurements were performed using an Oxford Instruments Optistat DN liquid nitrogen cryostat placed in the beam path of a Shimadzu UV-vis spectrometer. The PYP sample was dissolved in a solution of 66% glycerol and 33% water in a custom designed cell. The procedure for cryokinetic experiments has been described in detail elsewhere[59] and is very similar to cryotrapping. The sample is cooled to the proper temperature and a reference spectra is collected. Then the sample is illuminated for ~30 minutes with the selected pump wavelength to initiate the photocycle and absorption spectra are collected again. The difference between the reference spectra and the illuminated spectrum at the same temperature are calculated to eliminate the influence of thermal equilibration and create spectra that resemble ultrafast transient absorption spectra for ease of interpretation.

Ultrafast DEWI-PP absorption. The dispersed transient absorption setup was constructed from an amplified Ti:Sapphire laser system (Spectra Physics Spitfire Pro and Tsunami) operating at 1-kHz, which produced 2.25-mJ pulses of 800-nm fundamental output with a 40-fs (Full Width at Half Maximum) duration.[59, 65, 69, 70] The 800-nm fundamental pulse train was split into multiple paths with one path generating the dispersed white-light probe supercontinuum (350 – 650 nm) by focusing the laser pulses into a slowly translating CaF_2 crystal. Two other paths were used to generate the 435-nm and 475-nm tunable visible pulses (~250 nJ) from a home-built non-collinear optical parametric amplifier (NOPA) which are impinged and overlapped, both spectrally and temporally, on the sample. 435-nm and 475-nm pulses were selected to avoid contamination with solvated electrons.[35] The 435-nm and 475-nm pump beams were optically chopped at 500 Hz and 250 Hz, respectively, to generate a pulse sequence in which the reference spectrum and excited spectra were collected sequentially. The illuminated spectra share the same

reference spectra for the calculation of transient spectra. Both pump pulses were linearly polarized at 54.7^{o} (magic angle) with respect to the probe pulses. The spot size diameters (~300-μm pump pulse and 50-μm probe pulses) were estimated using a micrometer stage and razor blade. The appreciably greater diameter of the pump pulse minimizes artificial contributions to the signals from a varying spatial overlap between pump and probe beams. The PYP sample was circulated through a custom 1-mm path length flow cell with 0.2 mm thick quartz windows. The overall instrument response was 125 fs as measured by the signal rise time.

Computational Analysis. Initial structure of the Hhal PYP protein was taken from the PDB databank code 2ZOH.[71] After addition of the missing hydrogens, the protein molecule was solvated in a 6x6x6 nm periodic cube of water with 6 Na^{+} ions to neutralize the system. The total system contained 25,174 atoms. The protein geometry was minimized for 10,000 steps followed by a molecular dynamics equlibration for 20 ns with 2 fs time steps using an NPT ensemble at pressure of 1 bar[72] with a 1ps time constant for pressure coupling and compressibility of 4.5 x 10^{-5} bar^{-1} and temperature of 300K,[73] with a 0.1 ps time constant for the temperature coupling. The LINCS algorithm was used to constrain bond length[74], allowing a time step of 2 fs in the classical simulations. SETTLE was applied to constrain the internal degrees of freedom of the water molecule[75] A 1.0 nm cut-off was used for non-bonded Van der Waals' interactions, which were modeled by Lennard-Jones potentials. Coulomb interactions were computed with the smooth particle mesh Ewald method[76], using a 1.0 nm real space cut-off and a grid spacing of 0.12 nm. The relative tolerance at the real space cut-off was set to 10^{-5}. After equilibration, a full dynamics run for 100 ns with 2 fs time step was performed using the same NPT ensemble. All

structure preparations and molecular dynamics simulations were performed with the GROMACS software package[77] and parameters from the Amber03 force field with TIP3P model of water.[78]

From the production run, snapshots with different conformations of the R52 residue and T50 hydrogen bonding network around the *pCA* chromophore were extracted. A cluster, consisting of the protein molecule with a 5 Å layer of water around it, was cut from those snapshots and run through a full-scale QM/MM optimization. The quantum mechanical region consisted of the *p*CA chromophore molecule, C69 residue and sidechains of Y42, E46, T50 amino acids - 68 atoms in total. To estimate the effect of the R52 conformation on the excitation energies, the sidechain of that amino acid was later included into the QM region. The QM/MM interface between the GROMACS package and the GAMESS(US) quantum chemistry package[79] was employed to perform this optimization using density functional theory with the PBE0/cc-pVDZ[80] basis set and Amber03 force field. After optimization, the vertical excitation energies (VEE) were computed using second order eXtended Multi-Monfigurational Quasi-Degenerated Perturbation Theory (XMCQDPT2)[81] using a five-state averaged Complete Active Space Self-Consistent Field (CASSCF)[82] wavefunction as a reference. The active space in these CASSCF calculations included the 11 π-orbitals of the chromophore and 12 electrons (i.e. XMCQDPT2/SA(5)-CASSCF(12,11)/cc-pVDZ). The vertical excitation energies and oscillator strengths were computed with the Firefly 8.2 program.[83]

Results

Static Fluorescence. Hhal PYP is weakly fluorescent with fluorescence quantum yields (Φ_f) that are less than 0.5%, but exhibit a clear excitation-wavelength dependence in both the emission and excitation spectra (Figure 3). The emission maximum of Hhal PYP changes slightly as a function of excitation wavelength, with shorter excitation wavelengths producing shorter emission wavelengths (Figure 3A, B).

Excitation on the far blue edge of the absorbance spectrum at 370-nm generates emission at 490 nm, while 480-nm excitation produces an emission at 498 nm. The largest changes in peak position of the emission spectra occur upon excitation above 460 nm, on the red flank of the absorbance band. However, the shape, including bandwidth and shoulder, of the fluorescence emission spectra is largely independent of excitation wavelength (Figure 3A). The characteristics of the excitation spectrum measured at 490 nm (Figure 3C), provides further evidence for wavelength-dependent fluorescence. The excitation spectrum (red curve) is substantially broader than the absorbance spectrum (black curve) with clear enhanced amplitudes on the flanking edges.

The wavelength dependence of the fluorescence quantum yield (Φ_f) was determined in two ways. First, the excitation wavelength dependent amplitude of the emission peak was normalized to the sample absorbance. Secondly, the measured excitation spectrum of Hhal PYP was divided by its absorbance spectrum. Both approaches yield near identical results (Figure 3C; unfilled circles). The value of Φ_f is smallest near 450 nm and increases upon excitation with light on both the blue flank and red flank of the Hhal PYP absorbance band. Hence, both higher energy, 400 nm, and lower energy excitation, 480 nm, result in up to twice as much emission as excitation at the pG absorbance peak, 440 nm. Since the observed dependence of fluorescence quantum yield on excitation wavelength resembles the absorbance spectrum, we performed additional measurements at multiple reduced sample concentrations, demonstrating that inner filter effects did not contribute to the fluorescence yields in Figure 3C (data not shown).

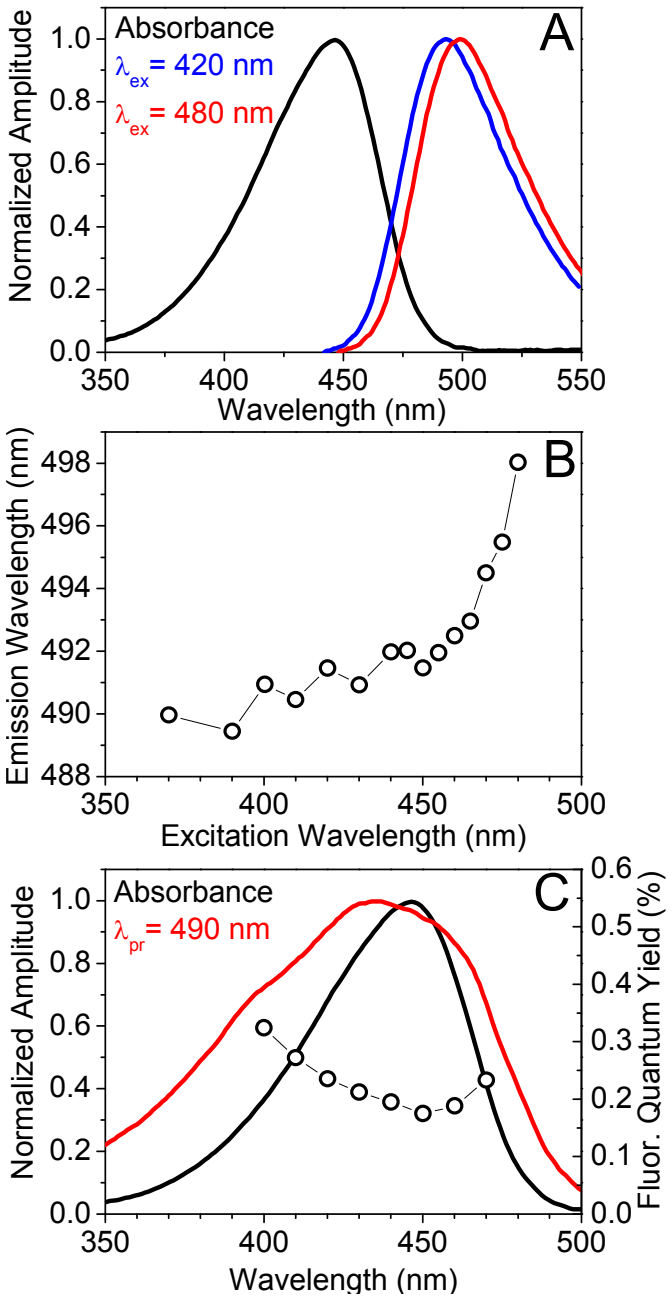

Figure 3: Wavelength dependence of the fluorescence quantum yield for wild type PYP. A: Absorbance spectrum of PYP (black) and emission spectra resulting from excitation of PYP at 420 nm (blue) and 480 nm (red). B: Emission peak wavelength as a function of excitation wavelength. C: Comparison of the absorbance (black) and fluorescence excitation spectra (red) of Hhal PYP. The quantum yield for fluorescence as a function of excitation wavelength is depicted (open circles, scaled according to right y-axis). These data were obtained by measuring emission spectra at several different wavelengths and normalizing for the amount of absorbed

light. The dotted line shows the values obtained by dividing the excitation and absorbance spectra.

Cryotrapping Spectra. The full cryokinetic spectra and analysis of Hhal PYP was published previously.[59] Here we focus on the excitation wavelength dependence of the difference spectra at only two temperatures, 90 K and 170 K. Upon 405 nm illumination at 90 K the spectra display a positive I_0 photoproduct band at 500 nm and a possible pUV photoproduct at 375 nm . The Ground State Bleach has multiple peaks at 455 nm, 425 nm and a shoulder at 400 nm (Figure 4A). Immamoto and coworkers[20] also observed multiple GSB signals in their low temperature spectroscopy. Under illumination with a different laser diode at 445 nm at 90 K, I_0 is still present, with no clear of pUV state and with altered relative amplitudes of the multiple GSB signals. Illumination with 405 nm results in lower I_0 signals and a more intense bleach at 425 nm, while 445 nm illumination results in a larger I_0 band with a smaller 425 nm bleach feature. These data indicate that illumination at different wavelengths is manipulating subpopulations of the Hhal PYP ground state that cannot interconvert because of the low thermal energy available. 405 nm illumination favors the 425 nm subpopulation and contributes less to I_0 photoproduct formation while 445 nm illumination favors the 455 nm subpopulation with more I_0 photoproduct formation. 405 nm illumination may also favor the 400 nm subpopulation but the small shoulder does not have sufficient definition in the spectra to make an evaluation. At 90 K there is a clear wavelength dependence with at least two separate GSB subpopulations and different I_0 evolution.

The photocycle evolves as the temperature is raised to 170 K and the cryotrapping spectra under each illumination wavelength are now essentially identical. At this temperature the pR state is beginning to form with a peak at 475 nm and the pUV state at 375 nm is decaying. The GSB still displays some asymmetry with a shoulder at 425 nm but the shape of bleach after 405

nm radiation compared with 445 nm radiation are equal. The initial excitation wavelength dependent spectra of the Hhal PYP photocycle is not present at higher temperatures further along the photocycle.

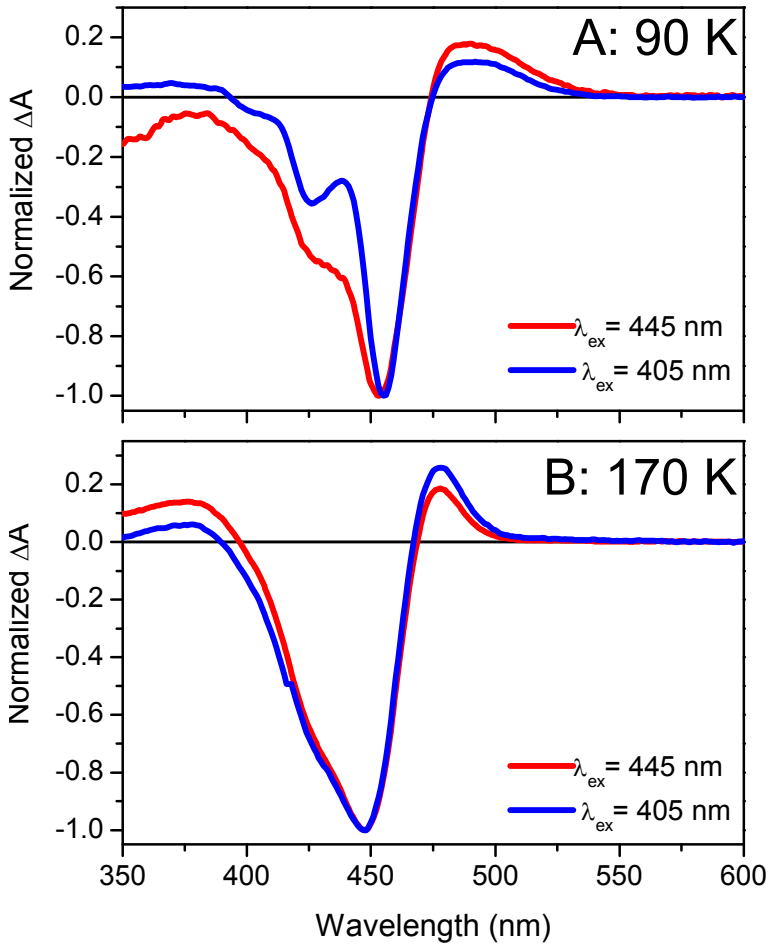

Figure 4: Cyrotrapped spectra at two temperatures (A: 90K and B: 170K) after illumination with 445 nm light (red curves) and 405 nm light (blue curves). The obvious differences in the I_0 feature at 500 nm and the GSB between the two pump wavelengths at 90 K are not present after evolution of the photocycle at 170 K. Wavelength dependent processes only influence the early stages of the photocycle.

Primary Photodynamics. Both datasets in the DEWI-PP signals produced by 435 nm and 475 nm excitation exhibit qualitatively similar features as in previously published data on Hhal PYP WT.[28, 35, 49, 59] To quantitatively compare the transient dynamics initiated from the two excitation

wavelengths, the spectra of both datasets were scaled to the bleach region from 400 nm to 450 nm in the terminal 6 ns spectrum. The spectra (Figure 5A) of the 435-nm excitation (blue) and 475-nm excitation (red) initially exhibit a ground-state bleach (GSB) between 400 nm and 475 nm with an excited-state absorption (ESA) in the range 340-400 nm and a stimulated emission (SE) in the range 450-600 nm. The ESA and SE signals for the 475 nm excitation are slightly higher, indicating that a greater proportion of the sample was excited with respect to the terminal population amplitude (Figure 5A,B). The GSB in the 475 nm excitation spectra is also noticeably red-shifted compared to the 435 nm excitation spectra at early probe times.

By 60 ps (Figure 5F), the amplitude differences in the ESA and SE have converged with formation of the I_0 photoproduct; spectra from both excitation wavelengths are nearly identical, including the GSB. This finding agrees with the cryotrapping analysis where initial differences in GSB spectra with different excitation wavelengths evolve into a single GSB shape. At 1.2 ns the spectra have diverged as the amplitude of the I_0 state (near 500 nm) is slightly larger upon 475 nm excitation than that for 435 nm excitation (Figure 5G). For the 6 ns spectra (Figure 5H), the GSB signal amplitudes are normalized from 400 nm to 450 nm, suggesting equal coexisting populations, but with different pR contributions.

Both DEWI-PP signals exhibit triphasic excited-state kinetics (Figure 6), mirroring observations from Hhal PYP WT transient absorption data measured previously.[13, 33-35, 49, 59] The ESA kinetics at 375 nm (Figure 6A) exhibit a greater amplitude in the 475 nm (red curve) excitation compared to the 435 nm (blue curve) for the duration of the experiment. The slight positive signal in the ns regime is likely due to the pUV state recently reported for Hh-PYP and other PYPs,[59, 70] but this state does not emerge from further global analysis, because of its very low level of accumulation. The 450 nm GSB trace (Figure 6B) exhibits an initial deeper bleach

in the 475 nm excitation and the convergence of the two excitation signals around 100 ps. The 510 nm (Figure 6C) and 550 nm (Figure 6D) traces the SE signals decay into a similar positive I_0 signal at ~10 ps, followed by a decay as I_0 evolves into the blue-shifted pR population at ~300 ps.

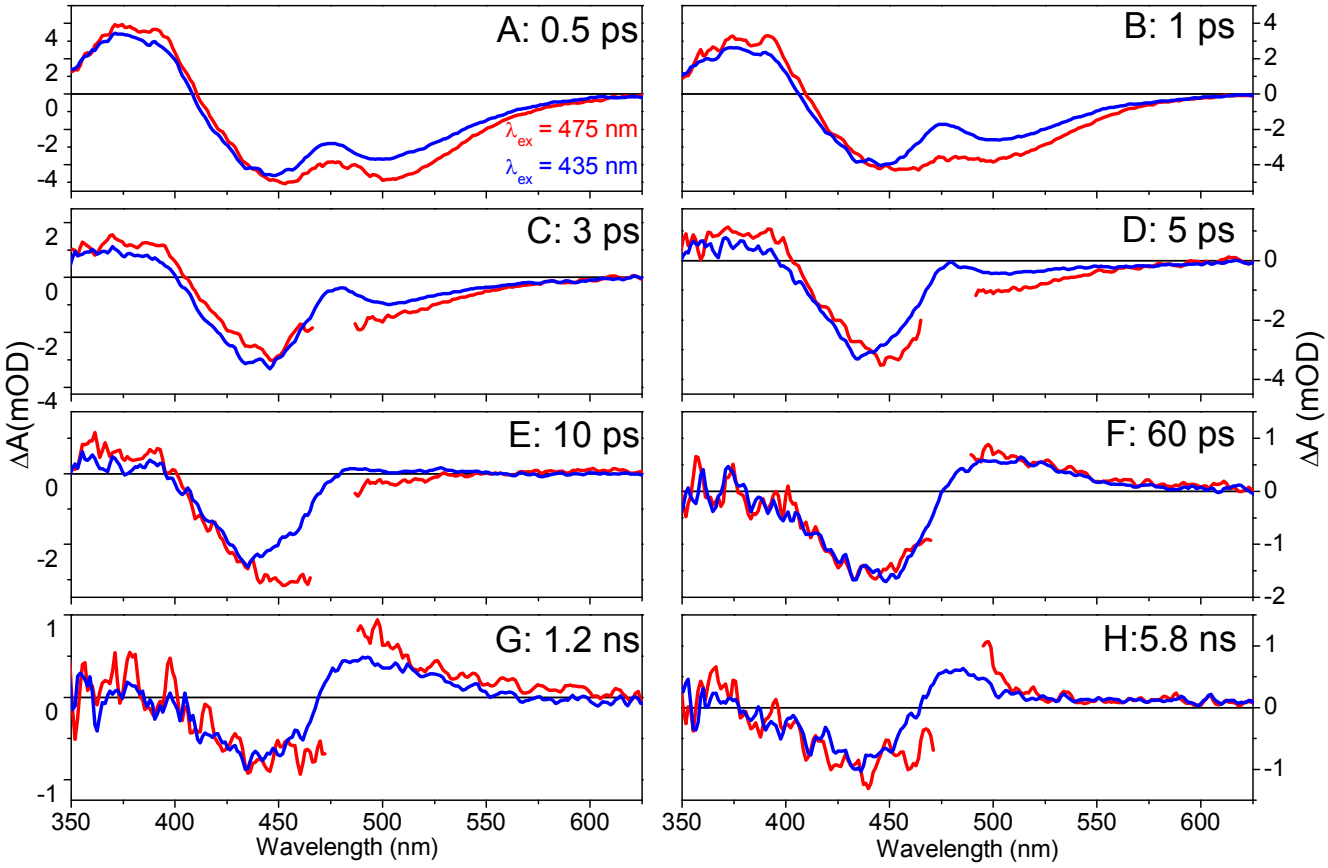

Figure 5. Comparison of select transient spectra from 435-nm excitation (blue) and 475-nm excitation (red) at selected probe times as indicated. Removed regions of the 475-nm excitation spectra are due to excessive pump scattering; the 435-nm dataset did not exhibit significant scattering to warrant excising data. Panels A and B clearly illustrate the pG* spectra of HhaI PYP with ESA, GSB and SE signals. Panels C and D show the decay of the pG* state and the red shifted GSB upon 475 nm excitation. In panels E and F the I_0 state is formed and blue shifts in panel G into the last observed pR photoproduct in panel H. The spectra were normalized for comparison at 6 ns from 400 to 450 nm.

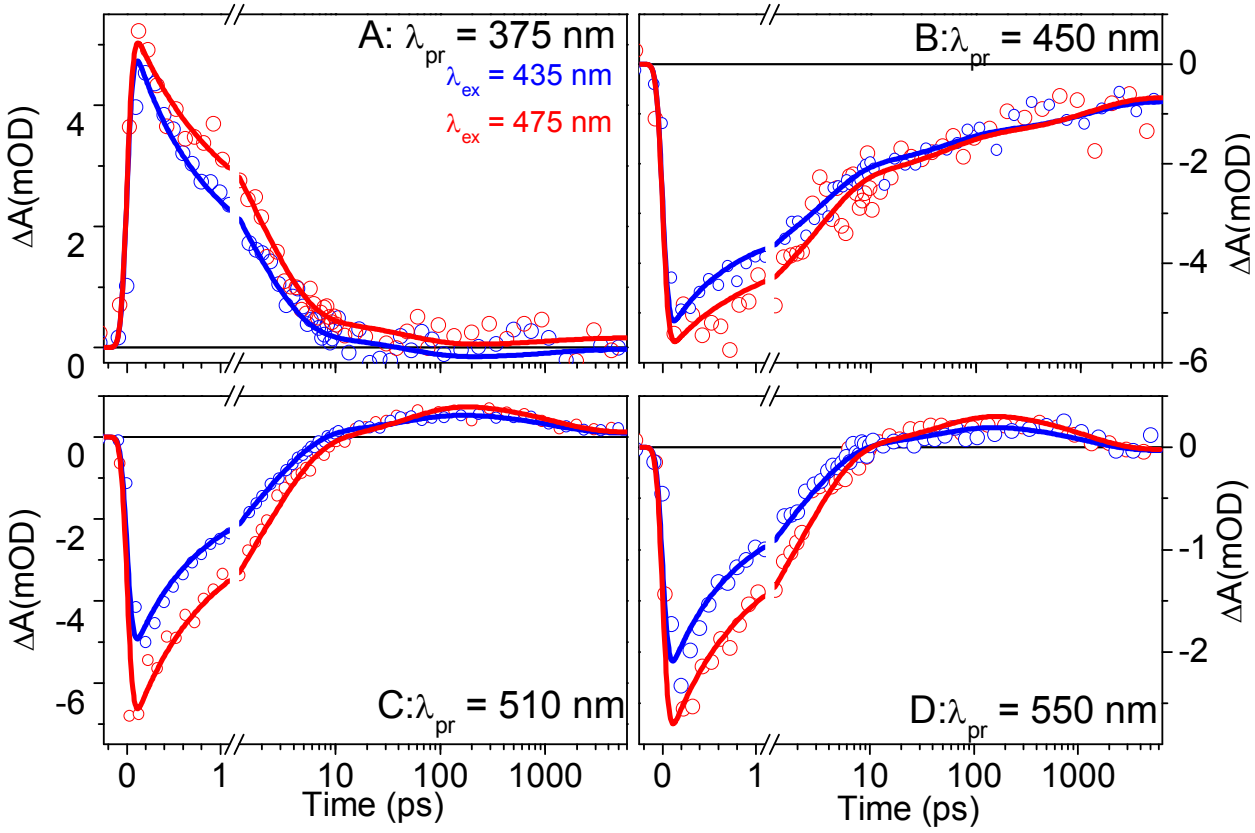

Figure 6: Kinetics (open circles) for 435-nm excitation (blue) and 475-nm excitation (red) at specific wavelengths with the global analysis fits (line). Panel A) illustrates the ESA decay, panel B) the GSB, panel C) is the evolution from SE to I_0 to pR, and panel D) displays largely SE kinetics with some I_0 influence. As with the spectra in Figure 5, the data was normalized for comparison at 6 ns from 400 to 450 nm. Figure S1 and S3 compare the kinetics across the probed wavelengths.

Global Analysis

Multicompartment global analysis techniques were used to quantitatively describe the ultrafast signals for the both excitation wavelengths.[84,85] Multiple kinetic models were created and evaluated based on their ability to represent a plausible molecular mechanism, and their simplicity. If a model is the true representation of the mechanism, then the extracted Species Associated Difference Spectra (SADS) are the "correct" spectra of the constituent populations; if inaccurate, the SADS represent a linear combination of the spectra of the real species. In this effort, two models were developer based on models that were developed for PYP previously.[35,

[49, 86, 87] The first model (Figure 7) has three heterogeneous ground states which are excited to pG* and may relax into a short lived Ground State Intermediate (GSI) population before returning to the pG ground state or evolve to produce I_0 and pR. The second model (Supporting Information Figure S1B) has two heterogeneous ground states that vibrationally relax and isomerize on comparable timescales.

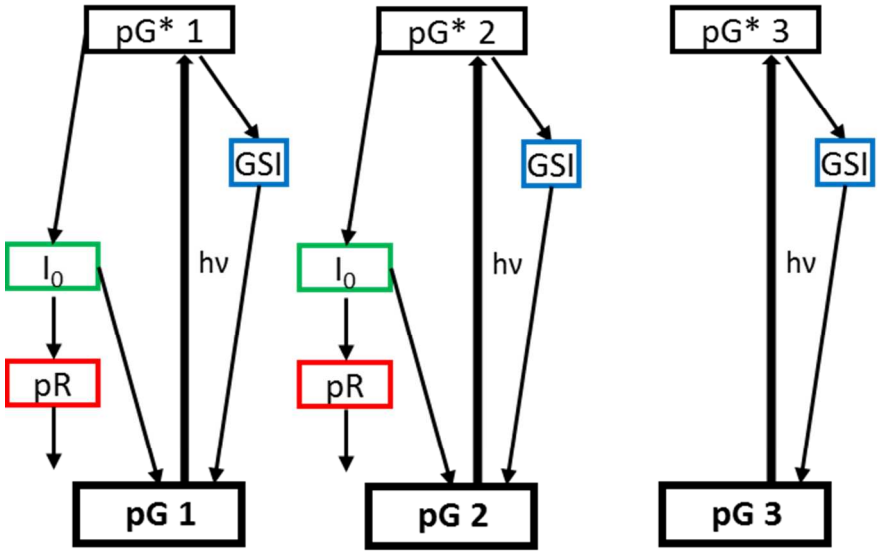

Figure 7: Three state heterogeneous global analysis model in to fit the transient absorption dynamics from each DEWI-PP dataset were the same different parameters. The excitation wavelength dependent shows up in the spectral features of the extracted SADS from the fits.

Both global models fit the dynamics of Hhal PYP excitation nearly identically with a root mean squared fit error of 0.909 and 0.896 a difference of 1.4%. In each model the kinetics of the 435 nm and 475 nm are fitted with the same kinetics parameters and the wavelength dependent differences are resolved in the corresponding SADS spectra. While both models include inhomogeneity to explain the DEWI-PP data, the three-state heterogeneous model is preferred for its simplicity and its prediction of an excitation wavelength dependent to the initial kinetics that were not observed in the data. Hence, the remainder of the discussion will focus on the

application of the three-state inhomogeneity model in Figure 7, however for completeness of the discussion, the kinetic parameters and spectra for the two state vibrational relaxation model are given in the supporting information (Table S2, Figure S4 and S5).

Within the inhomogeneous model in Figure 7, both DEWI datasets are fit to the same similar triphasic pG* quenching kinetics with 1.1 ps, 4.7 ps, and 34 ps lifetimes (Table 1 and Figure 7 black boxes). As demonstrated below, the DEWI datasets can be fit with the same decay time constants, but with differing amplitudes and spectra. While previous studies[35, 48, 59] on Hhal PYP WT assumed that each pG* population was spectrally identical with different kinetic time constants, the raw DEWI-PP data in Figures 4 and 5 clearly show that 435 nm and 475 nm excitation produce similar, albeit not identical, pG* spectra. Thus the SADS of the constituent pG* states must be different in the modeling. The SADS of the fastest and intermediate pG* populations were unconstrained in the global analysis fitting, while the weak-amplitude third population was locked to the second. The ESA features in all the pG* spectra are identical both among and between excitation wavelengths. In all the pG* GSB features excitation at 475 nm versus excitation at 435 nm produces a red shifted bleach by about ~10 nm. All the 475 nm excitation pG* states also produce greater amplitude SE signals than in the 435-nm excitation signals compared to the GSB. This suggests the higher fluorescence yield (Figure 3C) observed after 475 nm excitation versus 435 nm excitation may result in part by an increased oscillator strength and changing quantum yields. Within a single excitation wavelength there are slight differences in the SE regions of the different heterogeneous pG* states. Under 435 nm illumination the pG* 1 SE at 500 nm produces a more rounded gradual peak than at later times in pG*2&3. Under 475 nm illumination the SE is blue shifted slightly and forms a sharper peak

than in pG*2&3. These differences are more evident when the pG* spectra are overlapped as seen in the Supporting Information (Figure S3).

Table 1: Global Analysis Parameters of the DEWI datasets. These are optimized by target analysis to the model in Figure 7 for Hhal PYP after 435-nm and 475-nm excitation.

State	pG* 1	pG* 2	pG* 3	GSI	I_0	pR
			Heterogeneous Larsen Model			
Population (%)	**57**	**32**	**11**			
Lifetime (ps)	1.1	4.7	34	4.5	970	∞
Branching Yields (%)	67 (GSI) 33 (I_0)	67 (GSI) 33 (I_0)	100 (GSI) 0 (I_0)		35 (pG) 65 (pR)	
pR Yield (%)	14	8	0			Total - 22

Relative error for each parameter is 10%.

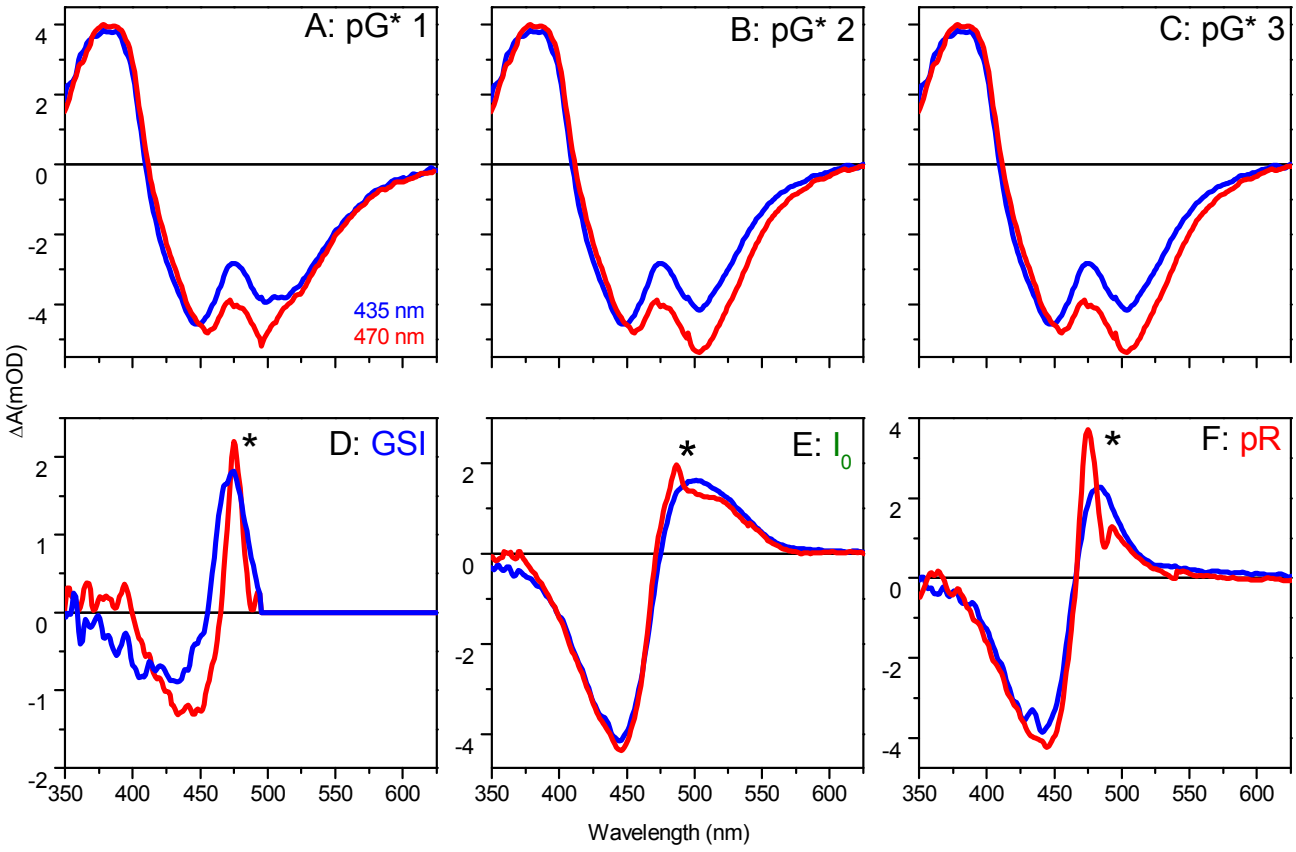

Figure 8: Comparison of Global Analysis SADS for 435-nm excitation (blue) and 475-nm excitation (red)**.** Spectra are calculated from the transient absorption spectra which were normalized at 6 ns between 400 and 450 nm. The target model and concentration profiles correlated with these SADS are shown in Figure 7. Panels A, B and C show the SADS for the three heterogeneous pG* states. In panels B and C the red shift of the GSB in 475 nm excitation is evident. The GSI spectra and the extremely clear difference in the GSB at early times is shown in panel D. The I_0 intermediate SADS is in panel E and the later pR photoproduct SADS in panel F where the GSBs are approximately identical. The sharp starred peaks in panels D, E, and F are due to scattering of the 475 nm excitation light into the detector.

Quenching of pG* populations proceed through a Ground State Intermediate[35] (GSI) (Figure 8D and Figure 7, blue boxes) that is argued from pump-dump-probe spectroscopy to be a highly vibrationally excited electronic ground state species which is produced when the *p*CA chromophore fails to enter the photocycle and non-radiatively relaxes.[35] The transient GSI spectra are red-shifted from the GSB peaking at 470 nm. The GSI spectrum for 475 nm excitation clearly shows the red shifting of the GSB spectra at early times compared to the 435 nm excitation GSB.

The DEWI-PP data indicate that the heterogeneity of the excited-state pG* populations may not propagate through the first two intermediates of the resulting photocycle dynamics. The I_0 (Figure 8E) state exhibits slight kinetic and spectral differences depending on the excitation wavelengths, but the main indicator of heterogeneity, the GSB, is almost identical. The recombination of the bleach spectra at later probe times matches the cryotrapping experiments which showed the GSB differences also recombined at higher temperatures (Figure 4). The pR SADS (Figure 8F) with 475 nm excitation does produce slight larger bleach at the peak, however the GSB region as a whole is similar.

The photoproduct quantum yields Φ_{ph} were evaluated from the populations and branching ratios modeled in our global analysis (Table 1). In agreement with previous PYP studies,[35, 49, 59, 87] the overall pR yield is 22% and the primary contributor to the production of I_o and pR is the fastest pG* 1 state. Since both excitation wavelengths are fit to the same model to make the spectral differences clear, we did not calculate any differences in the quantum yield under 435 nm or 475 nm excitation.

Discussion

While the differences between 435 nm and 475 nm excitation are small, they are well resolved in the DEWI-PP measurements. The primary photodynamics, cryotrapping spectra, and fluorescence dynamics of PYP are clearly manipulated by excitation wavelength. Three hypotheses are considered for the origin of this effect (Figure 9): (1) The Multiple Electronic Excited-State Model, (2) The Vibrationally Enhanced Isomerization Model, and (3) The Static Heterogeneity Model.

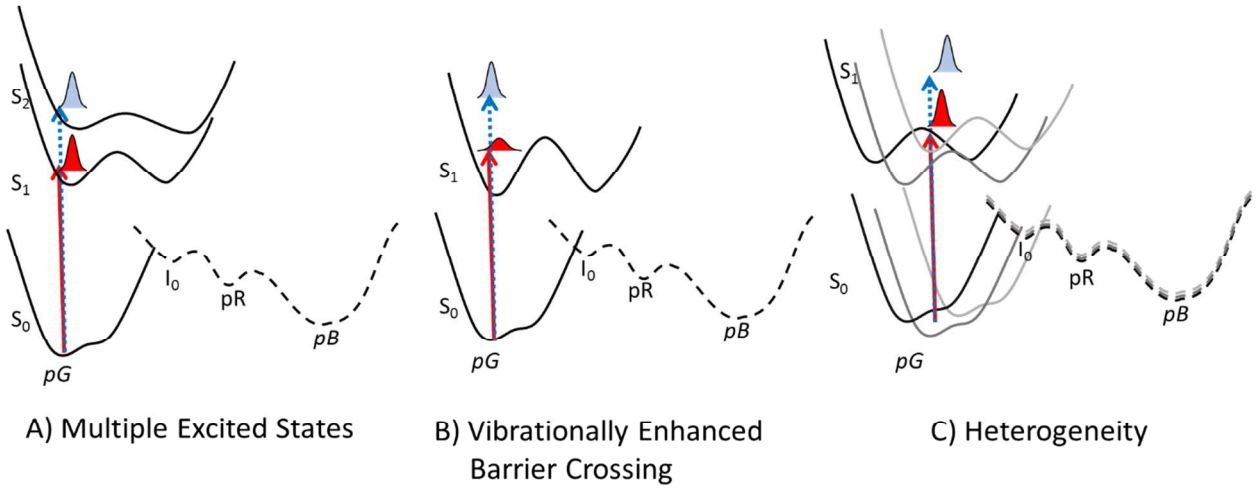

Figure 9: Depiction of three models conceived to explain excitation-wavelength dependence in PYP. Panel A: Multiple Electronic Excited-State Model, Panel B: Vibrationally Enhanced Isomerization, and Panel C: Static Heterogeneity.

The Multiple Electronic Excited-State Model: This model hypothesizes that the pG spectrum of Hhal PYP is attributed to a single homogeneous population with two or more overlapping absorption bands attributed to different electronic transitions (Figure 9A). Excitation to different excited-state potential energy surfaces will affect the nature of the intersections with the ground-state, leading to different photodynamics. Other photochemical systems like azobenzene[88] and metal carbonyls[89] are known examples of multiple electronic excited states influencing photochemistry.

If excitation into different excited electronic states of PYP (Figure 9A) resulted in differing photodynamics, then the fluorescence, cyrotrapping, and DEWI signals would certainly exhibit an excitation wavelength dependence. Quantum calculations[90, 91] that include the local amino acid environment predict a large energy gap (≥ 1 eV) between S_1 ($\pi\rightarrow\pi^*$) and S_2 ($n\rightarrow\pi^*$) that places the $n\rightarrow\pi^*$ transition out of reach of the wavelengths in this DEWI-PP experiment (435 nm, 2.8 eV; 475 nm, 2.6 eV). There is evidence for multiple excited states influencing the isomerization of the neutral pCA chromophore in the gas phase[92] but subsequent efforts have questioned this result.[93]

Multiple excited states are consistent with some aspects of the Hhal PYP dynamics. The observed fluorescence spectra exhibit red shifting with excitation wavelength (Figure 3B) consistent with multiple excited states where excitation on the red edge excites a pG* state at lower energy. The gradual fluorescence peak shift opposed to a large discreet jump requires multiple pG* populations close in energy. In the DEWI-PP measurements, differences between the triphasic pG* decay at different excitation wavelengths can be interpreted using three pG* states. Each of the multiple pG* states has its own spectral form and decay constants for transition to the ground state.

The multiple excited states model additionally predicts a homogeneous single GSB that is excitation wavelength independent. This is inconsistent, however, with the multiple bleach subpopulations observed in the cryotrapping spectra and ultrafast transient absorption experiments. At low temperature excitation at 405 nm produces obvious shifts towards a 425-nm bleach subpopulation compared to excitation at 445 nm (Figure 4). In the ultrafast experiments 435 nm excitation produces a blue shifted bleach, while 475 nm excitation produces a red shifted

bleach. Hence, while this hypothesis is able to explain the pG* triphasic decay and fluorescence emission, it is not sufficient for the wavelength dependent behavior of the GSB.

The Vibrationally Enhanced Isomerization Model: This model postulates that the photoisomerization behavior of Hhal PYP is ascribed to a homogeneous population with an electronic excited-state manifold with multiple vibronic levels which result in differing isomerization dynamics (Figure 9B). Photoexcitation launches a wave packet on this potential energy surface based on the amount of vibrational energy deposited by excitation (above the 0-1 transition energy). The excitation wavelength dependence of stilbene photoisomerization is heavily influenced by vibrational motion along the isomerization coordinate[94] increasing the rate and quantum yield in solution compared to the gas phase. The barrierless isomerization in rhodopsin is also wavelength dependent due to excited state vibrational wave packets,[95] with a significant drop in yields above 500 nm. For a vibrationally enhanced isomerization model to significantly affect the isomerization dynamics, the timescale of photoproduct formation must be comparable to vibrational relaxation. Due to the relative short dephasing time of less than ps, here, only the fastest decay component could be modulated due to vibrational enhancement.

If Hhal PYP is influenced by purely vibrationally enhanced barrier crossing, higher energy excitation should have significant effects on the photodynamics by allowing easier barrier crossing to produce faster excited state kinetics, greater photoproduct yields, and less fluorescence. Excitation at shorter wavelengths and higher vibrational energies are predicted to have higher photoproduct yields and lower fluorescence and longer wavelengths with lower vibrational energies have lower photoproduct yields and higher fluorescence. GSB and

photoproduct spectra and kinetics should be identical regardless of excitation wavelength in the vibrational enhanced barrier crossing model with a single ground state potential surface.

The observed fluorescence, cryotrapping, and transient spectra both deviate from the predictions by a pure vibrationally enhanced barrier crossing model. The curious shape of the fluorescence quantum yields (Figure 3C) with a minimum at 440 nm and maxima at 400 nm and 475 nm is not consistent with the steady increase in fluorescence at longer wavelengths predicted by a vibrational enhancement model. However, as with the multiple excited states model, the obvious differences in the GSB and photoproduct spectra are not consistent with a single ground state. For the red shifted bleach under 475 nm excitation to be the result of only Stokes shifting, the vibrational relaxation time would need to be around 100 ps, implausibly slow. Stokes shifting may be responsible for the red shift in the SE band at early times (Figure 5 A, B), but any differences in the GSB bleach caused by the Stokes shift would not persist later in the experiment. Furthermore, at 90 K the thermal energy available to produce vibrational effects is greatly decreased and at least two obvious ground state subpopulations are observed in the cryotrapping spectra. As with the multiple excited state model, vibrationally enhanced barrier crossing can explain some aspects of the pG* kinetics and quantum yields of the wavelength dependence, but does not describe the wavelength dependent ground state bleach.

The Static Heterogeneity Model: This model argues that the absorption spectrum of Hhal PYP can be ascribed to a single S_1 excited state, but that multiple subpopulations coexist due to functionally relevant variations in protein environment (Figure 9C). The heterogeneous mechanism predicts that the primary photochemistry varies with excitation wavelength because

it is possible to selectively excite different subpopulations that exhibit differing intrinsic photodynamics.

The static heterogeneous model combines features of multiple pG* excited states with multiple ground states. In the heterogeneous system, each ground state and each excited state can have a different potential energy surface with a different energy separation and different fluorescence spectra. The wavelength dependence in both the Hhal PYP fluorescence emission spectra and fluorescence quantum yield (Figure 3) indicate that excitation at 400 nm, 446 nm and 480 nm are sampling different portions of the pG* surface with different local minima and different fluorescence energies. The first pG* subpopulation exhibits a relatively high fluorescence quantum yield (near 0.3%) and a relatively blue-shifted emission spectrum peak near 491 nm, the second subpopulation has a lower fluorescence quantum yield and an emission peak near 492 nm, and the third subpopulation has a somewhat higher fluorescence quantum yield combined with a red-shifted emission spectrum near 498 nm.

Cryotrapping spectra also support a heterogeneous model with two obvious subpopulations and a possible third. These subpopulations are evident at 90 K (Figure 4A) where the ground state bleach has two peaks at 455 nm, 425 nm and a possible shoulder at 400 nm. By altering the excitation wavelength the occupation of these ground state subpopulations can be manipulated and their influence on the initial I_0 photoproduct. Excitation at 445 nm results in a smaller 425 nm bleach and a larger I_0 amplitude implying that most of the photoproduct is formed by the 455 nm ground state.

The transient spectra in the DEWI datasets (Figures 5, 6) are also consistent with a three-state heterogeneous model. Transient spectra display multiple pG* states with different spectra and kinetic properties. The triphasic decay kinetics are best fit by a linear combination of three

exponential rates, representing the three heterogeneous pG* states. These pG* states also display spectral differences with the fastest population having a different SE features. Heterogeneity also provides the best framework for interpreting the wavelength dependent differences in the GSB and the photoproduct spectra. Excitation with 475 nm on the red edge of the absorption spectra preferentially excites the reddest heterogeneous population resulting in the red shift GSB spectra compared to 435 nm excitation.

The second model developed for PYP (Figure S1B) is a hybrid of the vibrational enhanced isomerization and static heterogeneity. The static heterogeneity is responsible for the shifts in the GSB and the vibrational relaxation contributes to the fit of the shifting SE signals observed at early times <10 ps (Figure S4 and 5). Attempts to assign the shifted GSB to the vibrational relaxation were not fruitful and any model explaining the GSB required heterogeneity. Vibrational relaxation may have a place in the dynamics of Hhal PYP but it is incapable of explaining all the observed wavelength dependence alone without the inclusion of heterogeneity. Heterogeneity is the simplest hypothesis available consistent with tri-phasic pG* decay, and wavelength dependent GSB bleaches.

Adoption of a heterogeneous model can explain aspects of the Hhal PYP photodynamics other studies have explained with more complicated models. Models with bifurcation[20, 52] following pG* to produce two different photoproducts can be expressed using two heterogeneous states each producing their unique product. Each heterogeneous pG* state has unique kinetic and spectral properties and they can produce varied photoproducts without bifurcation. Models with equilibria[51] can also be redrawn using heterogeneous states. Equilibria are mainly used to allow the production of primary photoproducts later in the photocycle. With heterogeneous states, primary photoproducts can be produced at different time scales in each pG* state. This allows for

the production of a photoproduct over an extended period of time without introducing equilibria. We believe that the heterogeneous model is the appropriate explanation for the Hhal PYP photodynamics.

*Heterogeneity in PYP***:** Heterogeneous Hhal PYP populations are likely created by variations in the positioning of the protein scaffold around the *p*CA chromophore.[96] Proteins are not static objects and in solution at physiological temperatures, they are dynamic, continually flexing and rotating, to sample different portions of the ground potential energy surface.[97] Variations in the hydrogen bonding network of the reversibly switchable fluorescent protein Dronpa[98] demonstrates structural heterogeneity can be a key element in protein photocycles. The origins of the observed heterogeneity in Hhal PYP have been examined by computational and NMR experiments exploring the conformations of R52 and T50 with respect to the *p*CA chromophore as potential heterogeneous agents.

R52 is in the chromophore binding pocket and shields *p*CA from solvent exposure in the folded pG state. The positive charge of arginine has been proposed to provide a counter-ion to the negative charge of the deprotonated chromophore, with a significant influence on the electronic potential energy surface of *p*CA and the subsequent excited-state dynamics.[99, 100] The charge of the R52 residue remains a subject of controversy as multiple structural studies have produce conflicting results. Yamaguichi et al[71] observed a neutral charge in their neutron diffraction studies, while earlier neutron diffraction studies by Moffat and coworkers[101] did not and the most recent crystallography effort by Kataoka[102] argues for both the cationic and neutral forms. NMR titration results by Mulder and coworkers posit that R52 is protonated in solution, which is probably more relevant to the *in vivo* action of Hhal PYP than crystals.[103] Further

support for a protonated R52 in the crystal comes from computer simulations that predicted an pKa upshift, rather than downshift for the R52 pKa in crystals.[104]

The R52Q mutant exhibits slower excited-state dynamics[105-107] and ~10% lower photocycle quantum yield than PYP (21%[108] vs. 25-35%), while the absorption spectrum is nearly identical to WT (446 nm). Solution NMR structures of the pG state place R52 in two configurations: either with the guanidinium group positioned directly above the phenol ring of *p*CA, or alternately with the guanidinium group positioned far from *p*CA and above Y98.[109] QM/MM calculations by Groenhof and coworkers[110] predict the guanidinium group is oriented either perpendicular or parallel to the *p*CA ring with a difference of up to 20 nm in the absorption spectra of pG based on the orientation. Further calculations using the Gromos96 force field solidify the influence of different conformers of R52 on the photocycle.[99, 110, 111]

New calculations using the Amber03 force field, presented here, have arrived at other possible conformers of R52 (Figure 10, Table 2). In the majority of the dynamics simulation R52 is observed in the perpendicular conformer with a torsion angle of +60° (Figure 10A), similar to the x-ray structure by Yamaguchi et al.[71] The R52 residue also samples a configuration with a torsion angle of -60° (Figure 10B), in line with the NMR structure determined by Bernard et al,[112] and rarely appears in the parallel conformer seen in the previous calculations.[110] Although the -60° R52 conformer is less populated than the +60° conformer, there are several transitions, and the -60° conformation has a lifetime that is significantly longer than the excited state lifetime of the chromophore (Table 2). The +60° and -60° conformers display differences in their electronic excitations with absorption at 454 nm and 439 nm (Table 2). Despite the differences in relative populations of the various R52 conformations, in simulations with both force fields, the wtPYP transitions from *trans*-pCA to *cis*-pCA along identical pathways.[60] All of these

conformers of R52 are qualitatively valid options for the positioning in the chromophore pocket and one mechanism that may be responsible for the heterogenous dynamics resolved in the flourescence, cryotrapping and DEWI data of Hhal PYP photodynamics.

T50 has also been identified as a possible source of heterogeneity in the chromophore pocket of Hhal PYP. The T50 residue is an important member of the hydrogen bonding network around the phenolate end of the pCA chromophore and any variations in its positioning would strongly influence the photodynamics. Crystallography and neutron diffraction results place T50 with a hydrogen bond to Y42 (Figure 11A). Computations performed by Ochsenfeld and coworkers[113] and confirmed in this work, demonstrate that T50 samples three different orientations with different hydrogen bond networks. First, T50 may hydrogen bond to Y42 as seen in the crystal structures (Figure 11A); Second, T50 may hydrogen bond to the carbonyl on the E46 backbone (Figure 11B); Third, T50 may hydrogen bond directly to the phenol of the *p*CA chromophore (Figure 11C). Ochsenfeld and coworkers[113] used these three conformers to calculate an accurate chemical shift for the E46 proton. In our simulations, these three conformers exchange on a picosecond timescale and have different electronic transitions. The T50-Y42 conformer transitions at 423 nm, the T50-E46 backbone conformer at 453 nm and the T50-pCA conformer at 426 nm (Table 2).

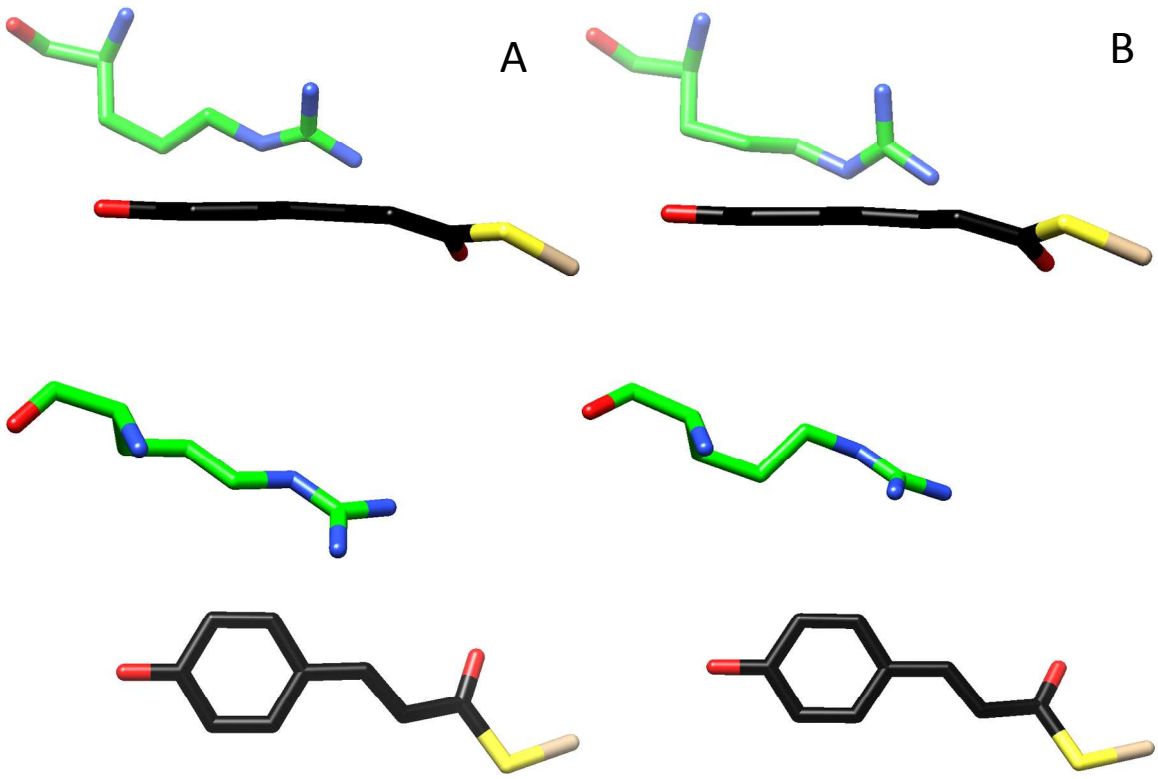

Figure 9: The +60° (A) and -60° (B) conformers of R52 (green) from calculations using the Amber3 force field in relation to the pCA chromophore (black) in the ground pG state.

Table 2: Possible Heterogeneous Conformers of PYP Revealed by QM/MM simulations

	R52*		**T50***		
Conformation	+60	-60	Y42	E46	pCA
Occupation Percentages (%)	97	3	12	10	78
Estimated Lifetimes (ps)	15 ns	160 ps	13 ps	14 ps	40 ps
Vertical Electronic Excitation (nm)	454	439	423	453	426

*See Figures 9 and 10 for structures.

Although these shifts are in line with the single configurational approximate coupled-cluster calculations of Ochsenfeld and co-workers,[113] our multi-configurational perturbation results suggest that the main absorption in solution is due to the configuration where T50 is hydrogen bonded with the E46 backbone (Figure 11B, Table 2). Excitation wavelength dependent excited state populations would be expected in Hhal PYP based on the T50 conformer population distribution at the moment of absorption. Collectively the variations in the calculated positions of T50 and R52 provide compelling evidence that there are ample degrees of freedom in the Hhal PYP chromophore pocket to produce excitation wavelength dependent heterogeneous ground states, excited states, and photoproducts.

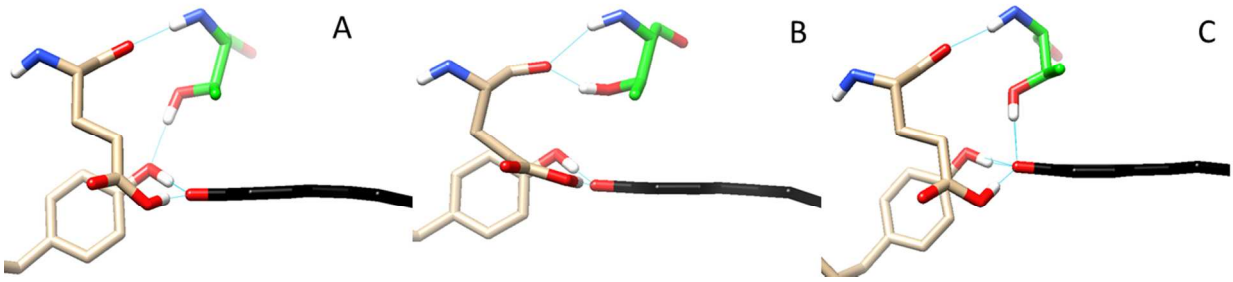

Figure 10: The three different conformers of T50 (green) in relations to the hydrogen bonding network around the pCA chromophore (black) in the ground pG state. In Panel A the T50 residue bonds with the Y42 alcohol (background); Panel B the T50 residue bonds with the E46 backbone carbonyl (foreground); and Panel C the T50 residue bonds with pCA (black).

Regardless of the origin, the wavelength-dependent heterogeneous Hhal PYP photodynamics requires reevaluation of the literature. Prior works paid little attention to the possible effect of wavelength dependence and the ability to compare experiments performed with different illumination light. It is expected that a greater range of excitation wavelengths than the 40 nm in this study (Figure 2) would exhibit more profound differences in the associated dynamics. Time

resolved crystallography by Anfinrud and coworkers[51] with a 390 nm pump, should be compared with reservations to crystallography by Ihee and coworkers[52] with an excitation pump at 418 nm and crystallography by Hutchinson and van Thor[114] with an excitation pump at 450 nm. Because any bulk sample represents a weighted average over all possible heterogeneous structures, different excitation wavelengths among the time resolved crystallographic structures[51, 52, 57, 60] create a different distribution of excited heterogeneous populations whose spectral, kinetic, quantum yield and structural properties are not equivalent. This same argument applies to any comparisons of techniques using different pump wavelengths (Figure 2 and Table S1) including: low temperature spectroscopy,[15, 20, 56, 59] visible ultrafast transient experiments,[49, 59, 87, 115] infrared observations,[29, 32] and fluorescence measurements.[21, 31, 116] Direct comparisons of PYP studies which have been performed using dissimilar pump wavelengths must be performed with caution and are not expected to have identical kinetic life times or spectra.

Concluding Comments

Wavlegnth dependent excitation of Hhal PYP with 475 nm light vs 435 nm light has a small, but measurable, effect on the fluorescence, cryotrapped spectra and ultrafast photodynamics. We would expect these effects to scale with excitation far from the 440 nm absorbance center to display the greatest deviations. Multiple excited state interactions, vibrationally enhanced barrier crossing, and pG heterogeneity are possible causes of the wavelength dependence. Heterogeneity in the ground, excited, and photoproduct states is the only model which can explain all of the differences, including the ground state bleaches, tri-phasic excited state quenching, photoproduct amplitudes, and quantum yields. Heterogeneity is likely created by the subtle movements of proteins in solution environments, and in PYP rotamers of R52 are a possible contributor.

Conformers of T50 resulting in variations of the hydrogen bond network have also been identified in new QM/MM calculations as possible heterogeneous residues. Confirmation of wavelength dependence in PYP encourages caution with all future and past comparisons between PYP studies with different excitation wavelengths.

Supporting Information

Supporting information for this work, including the table of excitation wavelengths in Hhal PYP WT studies, can be found online at: http://pubs.acs.org.

Acknowledgements

Dr. Mikas Vengris (Light Conversion Ltd.) is acknowledged for the donation of global and target analysis software package used initially in the analysis.

References

[1] Kumauchi, M., Hara, M. T., Stalcup, P., Xie, A., and Hoff, W. D. (2008) Identification of Six New Photoactive Yellow Proteins—Diversity and Structure–Function Relationships in a Bacterial Blue Light Photoreceptor, *Photochemistry and Photobiology 84*, 956-969.

[2] Meyer, T. E., Kyndt, J. A., Memmi, S., Moser, T., Colon-Acevedo, B., Devreese, B., and Van Beeumen, J. J. (2012) The growing family of photoactive yellow proteins and their presumed functional roles, *Photochemical & Photobiological Sciences 11*, 1495-1514.

[3] Hoff, W. D., Dux, P., Hard, K., Devreese, B., Nugteren-Roodzant, I. M., Crielaard, W., Boelens, R., Kaptein, R., Beeumen, J. V., and Hellingwerf, K. J. (1994) Thiol ester-linked p-coumaric acid as a new photoactive prosthetic group in a protein with rhodopsin-like photochemistry, *Biochemistry 33*, 13959-13962.

[4] Sprenger, W. W., Hoff, W. D., Armitage, J. P., and Hellingwerf, K. J. (1993) The eubacterium *Ectothiorhodospira halophila* is negatively phototactic, with a wavelength dependence that fits the absorption spectrum of the photoactive yellow protein, *Journal of Bacteriology 175*, 3096-3104.

[5] Horst, M. A. v. d., Stalcup, T. P., Kaledhonkar, S., Kumauchi, M., Hara, M., Xie, A., Hellingwerf, K. J., and Hoff, W. D. (2009) Locked Chromophore Analogs Reveal That Photoactive Yellow Protein Regulates Biofilm Formation in the Deep Sea Bacterium *Idiomarina loihiensis*, *Journal of the American Chemical Society 131*, 17443-17451.

[6] Kumar, A., Ali, A. M., and Woolley, G. A. (2015) Photo-control of DNA binding by an engrailed homeodomain-photoactive yellow protein hybrid, *Photochemical & Photobiological Sciences 14*, 1729-1736.

[7] Reis, J. M., and Woolley, G. A. (2016) Photo Control of Protein Function Using Photoactive Yellow Protein, In *Optogenetics: Methods and Protocols* (Kianianmomeni, A., Ed.), pp 79-92, Springer New York, New York, NY.
[8] Deisseroth, K. (2011) Optogenetics, *Nat Meth 8*, 26-29.
[9] Müller, K., and Weber, W. (2013) Optogenetic tools for mammalian systems, *Molecular BioSystems 9*, 596-608.
[10] Meyer, T. E., Yakali, E., Cusanovich, M. A., and Tollin, G. (1987) Properties of a water-soluble, yellow protein isolated from a halophilic phototrophic bacterium that has photochemical activity analogous to sensory rhodopsin, *Biochemistry 26*, 418-423.
[11] Cusanovich, M. A., and Meyer, T. E. (2003) Photoactive Yellow Protein: A Prototypic PAS Domain Sensory Protein and Development of a Common Signaling Mechanism, *Biochemistry 42*, 4759-4770.
[12] Hellingwerf, K. J., Hendriks, J., and Gensch, T. (2003) Photoactive Yellow Protein, A New Type of Photoreceptor Protein: Will This "Yellow Lab" Bring Us Where We Want to Go?, *The Journal of Physical Chemistry A 107*, 1082-1094.
[13] Ujj, L., Devanathan, S., Meyer, T. E., Cusanovich, M. A., Tollin, G., and Atkinson, G. H. (1998) New Photocycle Intermediates in the Photoactive Yellow Protein from *Ectothiorhodospira halophila*: Picosecond Transient Absorption Spectroscopy, *Biophysical Journal 75*, 406-412.
[14] Brudler, R., Rammelsberg, R., Woo, T. T., Getzoff, E. D., and Gerwert, K. (2001) Structure of the I1 early intermediate of photoactive yellow protein by FTIR spectroscopy, *Nat Struct Mol Biol 8*, 265-270.
[15] Xie, A., Kelemen, L., Hendriks, J., White, B. J., Hellingwerf, K. J., and Hoff, W. D. (2001) Formation of a New Buried Charge Drives a Large-Amplitude Protein Quake in Photoreceptor Activation, *Biochemistry 40*, 1510-1517.
[16] Pan, D., Philip, A., Hoff, W. D., and Mathies, R. A. (2004) Time-Resolved Resonance Raman Structural Studies of the pB′ Intermediate in the Photocycle of Photoactive Yellow Protein, *Biophysical Journal 86*, 2374-2382.
[17] Hellingwerf, K. J., Hendriks, J., and Gensch, T. (2002) On the Configurational and Conformational Changes in Photoactive Yellow Protein that Leads to Signal Generation in *Ectothiorhodospira halophila*, *Journal of Biological Physics 28*, 395-412.
[18] Hoff, W. D., Kwa, S. L. S., van Grondelle, R., and Hellingwerf, K. J. (1992) Low-Temperature Absorbency And Fluorescence Spectroscopy of the Photoactive Yellow Protein from *Ectothiorhodospira halophila*, *Photochemistry and Photobiology 56*, 529-539.
[19] van Brederode, M. E., Gensch, T., Hoff, W. D., Hellingwerf, K. J., and Braslavsky, S. E. (1995) Photoinduced volume change and energy storage associated with the early transformations of the photoactive yellow protein from Ectothiorhodospira halophila, *Biophysical Journal 68*, 1101-1109.
[20] Imamoto, Y., Kataoka, M., and Tokunaga, F. (1996) Photoreaction Cycle of Photoactive Yellow Protein from *Ectothiorhodospira halophila* Studied by Low-Temperature Spectroscopy, *Biochemistry 35*, 14047-14053.
[21] Chosrowjan, H., Mataga, N., Nakashima, N., Imamoto, Y., and Tokunaga, F. (1997) Femtosecond-picosecond fluorescence studies on excited state dynamics of photoactive yellow protein from *Ectothiorhodospira halophila*, *Chemical Physics Letters 270*, 267-272.
[22] Genick, U. K., Borgstahl, G. E. O., Ng, K., Ren, Z., Pradervand, C., Burke, P. M., Šrajer, V., Teng, T.-Y., Schildkamp, W., McRee, D. E., Moffat, K., and Getzoff, E. D. (1997) Structure of a Protein Photocycle Intermediate by Millisecond Time-Resolved Crystallography, *Science 275*, 1471-1475.
[23] Chosrowjan, H., Mataga, N., Shibata, Y., Imamoto, Y., and Tokunaga, F. (1998) Environmental Effects on the Femtosecond−Picosecond Fluorescence Dynamics of Photoactive Yellow Protein: Chromophores in Aqueous Solutions and in Protein Nanospaces Modified by Site-Directed Mutagenesis, *The Journal of Physical Chemistry B 102*, 7695-7698.

[24] Devanathan, S., Pacheco, A., Ujj, L., Cusanovich, M., Tollin, G., Lin, S., and Woodbury, N. (1999) Femtosecond spectroscopic observations of initial intermediates in the photocycle of the photoactive yellow protein from *Ectothiorhodospira halophila*, *Biophysical Journal 77*, 1017-1023.

[25] Masciangloli, T., Devanathan, S., Cusanovich, M. A., Tollin, G., and El-Sayed, M. A. (2000) Probing the primary event in the photocycle of photoactive yellow protein using photochemical hole-burning technique, *Photochemistry and Photobiology 72*, 639-644.

[26] Mataga, N., Chosrowjan, H., Shibata, Y., Imamoto, Y., and Tokunaga, F. (2000) Effects of Modification of Protein Nanospace Structure and Change of Temperature on the Femtosecond to Picosecond Fluorescence Dynamics of Photoactive Yellow Protein, *The Journal of Physical Chemistry B 104*, 5191-5199.

[27] Hanada, H., Kanematsu, Y., Kinoshita, S., Kumauchi, M., Sasaki, J., and Tokunaga, F. (2001) Ultrafast fluorescence spectroscopy of photoactive yellow protein, *Journal of Luminescence 94*, 593-596.

[28] Imamoto, Y., Kataoka, M., Tokunaga, F., Asahi, T., and Masuhara, H. (2001) Primary Photoreaction of Photactive Yellow Protein Studied by Subpicosecond-Nanosecond Spectroscopy, *Biochemistry 40*, 6047-6052.

[29] Imamoto, Y., Shirahige, Y., Tokunaga, F., Kinoshita, T., Yoshihara, K., and Kataoka, M. (2001) Low-Temperature Fourier Transform Infrared Spectroscopy of Photoactive Yellow Protein, *Biochemistry 40*, 8997-9004.

[30] Gensch, T., Gradinaru, C. C., van Stokkum, I. H. M., Hendricks, J., Hellingwerf, K., and van Grondelle, R. (2002) The Primary photoreaction of photoactive yellow protein (PYP): anisotropy changes and excitation wavelength dependence, *Chemical Physics Letters 356*, 347.

[31] Mataga, N., Chosrowjan, H., Shibata, Y., Imamoto, Y., Kataoka, M., and Tokunaga, F. (2002) Ultrafast photoinduced reaction dynamics of photoactive yellow protein (PYP): observation of coherent oscillations in the femtosecond fluorescence decay dynamics, *Chemical Physics Letters 352*, 220-225.

[32] Groot, M. L., van Wilderen, L. J. G. W., Larsen, D. S., van der Horst, M. A., van Stokkum, I. H. M., Hellingwerf, K. J., and van Grondelle, R. (2003) Initial Steps of Signal Generation in Photoactive Yellow Protein Revealed with Femtosecond Mid-Infrared Spectroscopy, *Biochemistry 42*, 10054-10059.

[33] Mataga, N., Chosrowjan, H., Taniguchi, S., Hamada, N., Tokunaga, F., Imamoto, Y., and Kataoka, M. (2003) Ultrafast photoreactions in protein nanospaces as revealed by fs fluorescence dynamics measurements on photoactive yellow protein and related systems, *Physical Chemistry Chemical Physics 5*, 2454-2460.

[34] Chosrowjan, H., Taniguchi, S., Mataga, N., Unno, M., Yamauchi, S., Hamada, N., Kumauchi, M., and Tokunago, F. (2004) Low-frequency vibrations and their role in ultrafast photoisomerization reaction dynamics of photoactive yellow protein, *Journal of Physical Chemistry B 108*, 2686-2698.

[35] Larsen, D. S., van Stokkum, I. H. M., Vengris, M., van der Horst, M. A., de Weerd, F. L., Hellingwerf, K. J., and van Grondelle, R. (2004) Incoherent Manipulation of the Photoactive Yellow Protein Photocycle with Dispersed Pump-Dump-Probe Spectroscopy, *Biophysical Journal 87*, 1858-1872.

[36] Vengris, M., van der Horst, M. A., Zgrablić, G., van Stokkum, I. H. M., Haacke, S., Chergui, M., Hellingwerf, K. J., van Grondelle, R., and Larsen, D. S. (2004) Contrasting the Excited-State Dynamics of the Photoactive Yellow Protein Chromophore: Protein versus Solvent Environments, *Biophysical Journal 87*, 1848-1857.

[37] Borucki, B., Otto, H., Meyer, T. E., Cusanovich, M. A., and Heyn, M. P. (2005) Sensitive circular dichroism marker for the chromophore environment of photoactive yellow protein: Assignment of the 307 and 318 nm bands to the n ->pi* transition of the carbonyl, *Journal of Physical Chemistry B 109*, 629-633.

[38] Heyne, K., Mohammed, O. F., Usman, A., Dreyer, J., Nibbering, E. T. J., and Cusanovich, M. A. (2005) Structural Evolution of the Chromophore in the Primary Stages of Trans/Cis Isomerization in Photoactive Yellow Protein, *Journal of the American Chemical Society 127*, 18100-18106.

[39] Ihee, H., Rajagopal, S., Šrajer, V., Pahl, R., Anderson, S., Schmidt, M., Schotte, F., Anfinrud, P. A., Wulff, M., and Moffat, K. (2005) Visualizing reaction pathways in photoactive yellow protein from nanoseconds to seconds, *Proc. Natl. Acad. Sci. U. S. A. 102*, 7145-7150.

[40] Vengris, M., Larsen, D. S., van der Horst, M. A., Larsen, O. F. A., Hellingwerf, K. J., and van Grondelle, R. (2005) Ultrafast dynamics of isolated model photoactive yellow protein chromophores: "Chemical perturbation theory" in the laboratory, *Journal of Physical Chemistry B 109*, 4197-4208.

[41] Espagne, A., Changenet-Barret, P., Plaza, P., and Martin, M. M. (2006) Solvent effect on the excited-state dynamics of analogues of the photoactive yellow protein chromophore, *J. Phys. Chem. A 110*, 3393-3404.

[42] van Stokkum, I. H., Gobets, B., Gensch, T., Mourik, F., Hellingwerf, K. J., Grondelle, R., and Kennis, J. T. (2006) (Sub)-picosecond spectral evolution of fluorescence in photoactive proteins studied with a synchroscan streak camera system, *Photochem Photobiol 82*, 380-388.

[43] van Wilderen, L. J. G. W., van der Horst, M. A., van Stokkum, I. H. M., Hellingwerf, K. J., van Grondelle, R., and Groot, M. L. (2006) Ultrafast infrared spectroscopy reveals a key step for successful entry into the photocycle for photoactive yellow protein, *Proceedings of the National Academy of Sciences 103*, 15050-15055.

[44] Nakamura, R., Hamada, N., Ichida, H., Tokunaga, F., and Kanematsu, Y. (2007) Ultrafast dynamics of photoactive yellow protein via the photoexcitation and emission processes, *Photochemistry and Photobiology 83*, 397-402.

[45] Nakamura, R., Hamada, N., Ichida, H., Tokunaga, F., and Kanematsu, Y. (2007) Coherent oscillations in ultrafast fluorescence of photoactive yellow protein, *The Journal of Chemical Physics 127*, 215102.

[46] Coureux, P. D., Fan, Z. P., Stojanoff, V., and Genick, U. K. (2008) Picometer-scale conformational heterogeneity separates functional from nonfunctional states of a photoreceptor protein, *Structure 16*, 863-872.

[47] Nakamura, R., Hamada, N., Ichida, H., Tokunaga, F., and Kanematsu, Y. (2008) Transient vibronic structure in ultrafast fluorescence spectra of photoactive yellow protein, *Photochemistry and Photobiology 84*, 937-940.

[48] Carroll, E. C., Hospes, M., Valladares, C., Hellingwerf, K. J., and Larsen, D. S. (2011) Is the photoactive yellow protein a UV-B/blue light photoreceptor?, *Photochemical & Photobiological Sciences 10*, 464-468.

[49] Rupenyan, A. B., Vreede, J., van Stokkum, I. H. M., Hospes, M., Kennis, J. T. M., Hellingwerf, K. J., and Groot, M. L. (2011) Proline 68 Enhances Photoisomerization Yield in Photoactive Yellow Protein, *The Journal of Physical Chemistry B 115*, 6668-6677.

[50] Nakamura, R., Hamada, N., Abe, K., and Yoshizawa, M. (2012) Ultrafast Hydrogen-Bonding Dynamics in the Electronic Excited State of Photoactive Yellow Protein Revealed by Femtosecond Stimulated Raman Spectroscopy, *The Journal of Physical Chemistry B 116*, 14768-14775.

[51] Schotte, F., Cho, H. S., Kaila, V. R. I., Kamikubo, H., Dashdorj, N., Henry, E. R., Graber, T. J., Henning, R., Wulff, M., Hummer, G., Kataoka, M., and Anfinrud, P. A. (2012) Watching a signaling protein function in real time via 100-ps time-resolved Laue crystallography, *Proceedings of the National Academy of Sciences 109*, 19256-19261.

[52] Jung, Y. O., Lee, J. H., Kim, J., Schmidt, M., Moffat, K., Šrajer, V., and Ihee, H. (2013) Volume-conserving trans-cis isomerization pathways in photoactive yellow protein visualized by picosecond X-ray crystallography, *Nature chemistry 5*, 212-220.

[53] Liu, J., Yabushita, A., Taniguchi, S., Chosrowjan, H., Imamoto, Y., Sueda, K., Miyanaga, N., and Kobayashi, T. (2013) Ultrafast Time-Resolved Pump–Probe Spectroscopy of PYP by a Sub-8 fs Pulse Laser at 400 nm, *The Journal of Physical Chemistry B 117*, 4818-4826.

[54] Naseem, S., Laurent, A. D., Carroll, E. C., Vengris, M., Kumauchi, M., Hoff, W. D., Krylov, A. I., and Larsen, D. S. (2013) Photo-isomerization upshifts the pKa of the Photoactive Yellow Protein chromophore to contribute to photocycle propagation, *Journal of Photochemistry and Photobiology A: Chemistry 270*, 43-52.

[55] Schmidt, M., Srajer, V., Henning, R., Ihee, H., Purwar, N., Tenboer, J., and Tripathi, S. (2013) Protein energy landscapes determined by five-dimensional crystallography, *Acta Crystallographica Section D 69*, 2534-2542.

[56] Zhu, J., Paparelli, L., Hospes, M., Arents, J., Kennis, J. T. M., van Stokkum, I. H. M., Hellingwerf, K. J., and Groot, M. L. (2013) Photoionization and Electron Radical Recombination Dynamics in Photoactive Yellow Protein Investigated by Ultrafast Spectroscopy in the Visible and Near-Infrared Spectral Region, *The Journal of Physical Chemistry B 117*, 11042-11048.

[57] Tenboer, J., Basu, S., Zatsepin, N., Pande, K., Milathianaki, D., Frank, M., Hunter, M., Boutet, S., Williams, G. J., Koglin, J. E., Oberthuer, D., Heymann, M., Kupitz, C., Conrad, C., Coe, J., Roy-Chowdhury, S., Weierstall, U., James, D., Wang, D., Grant, T., Barty, A., Yefanov, O., Scales, J., Gati, C., Seuring, C., Srajer, V., Henning, R., Schwander, P., Fromme, R., Ourmazd, A., Moffat, K., Van Thor, J. J., Spence, J. C. H., Fromme, P., Chapman, H. N., and Schmidt, M. (2014) Time-resolved serial crystallography captures high-resolution intermediates of photoactive yellow protein, *Science 346*, 1242-1246.

[58] Zhu, J., Vreede, J., Hospes, M., Arents, J., Kennis, J. T. M., van Stokkum, I. H. M., Hellingwerf, K. J., and Groot, M. L. (2015) Short Hydrogen Bonds and Negative Charge in Photoactive Yellow Protein Promote Fast Isomerization but not High Quantum Yield, *The Journal of Physical Chemistry B 119*, 2372-2383.

[59] Mix, L. T., Kirpich, J., Kumauchi, M., Ren, J., Vengris, M., Hoff, W. D., and Larsen, D. S. (2016) Bifurcation in the Ultrafast Dynamics of the Photoactive Yellow Proteins from *Leptospira biflexa* and *Halorhodospira halophila*, *Biochemistry 55*, 6138-6149.

[60] Pande, K., Hutchison, C. D. M., Groenhof, G., Aquila, A., Robinson, J. S., Tenboer, J., Basu, S., Boutet, S., DePonte, D. P., Liang, M., White, T. A., Zatsepin, N. A., Yefanov, O., Morozov, D., Oberthuer, D., Gati, C., Subramanian, G., James, D., Zhao, Y., Koralek, J., Brayshaw, J., Kupitz, C., Conrad, C., Roy-Chowdhury, S., Coe, J. D., Metz, M., Xavier, P. L., Grant, T. D., Koglin, J. E., Ketawala, G., Fromme, R., Šrajer, V., Henning, R., Spence, J. C. H., Ourmazd, A., Schwander, P., Weierstall, U., Frank, M., Fromme, P., Barty, A., Chapman, H. N., Moffat, K., van Thor, J. J., and Schmidt, M. (2016) Femtosecond structural dynamics drives the trans/cis isomerization in photoactive yellow protein, *Science 352*, 725-729.

[61] Rajagopal, S., Anderson, S., Srajer, V., Schmidt, M., Pahl, R., and Moffat, K. (2005) A structural pathway for signaling in the E46Q mutant of photoactive yellow protein, *Structure 13*, 55-63.

[62] Devanathan, S., Pacheco, A., Ujj, L., Cusanovich, M., Tollin, G., Lin, S., and Woodbury, N. (1999) Femtosecond spectroscopic observations of initial intermediates in the photocycle of the photoactive yellow protein from Ectothiorhodospira halophila, *Biophys J 77*, 1017-1023.

[63] Kim, P. W., Freer, L. H., Rockwell, N. C., Martin, S. S., Lagarias, J. C., and Larsen, D. S. (2012) Femtosecond Photodynamics of the Red/Green Cyanobacteriochrome NpR6012g4 from *Nostoc punctiforme*. 1. Forward Dynamics, *Biochemistry 51*, 608-618.

[64] Heyne, K., Herbst, J., Stehlik, D., Esteban, B., Lamparter, T., Hughes, J., and Diller, R. (2002) Ultrafast Dynamics of Phytochrome from the Cyanobacterium *Synechocystis*, Reconstituted with Phycocyanobilin and Phycoerythrobilin, *Biophysical Journal 82*, 1004-1016.

[65] Kim, P. W., Freer, L. H., Rockwell, N. C., Martin, S. S., Lagarias, J. C., and Larsen, D. S. (2012) Femtosecond Photodynamics of the Red/Green Cyanobacteriochrome NpR6012g4 from *Nostoc punctiforme.* 2. Reverse Dynamics, *Biochemistry 51*, 619-630.

[66] Larsen, D. S., Papagiannakis, E., van Stokkum, I. H. M., Vengris, M., Kennis, J. T. M., and van Grondelle, R. (2003) Excited state dynamics of beta-carotene explored with dispersed multi-pulse transient absorption, *Chemical Physics Letters 381*, 733-742.

[67] Imamoto, Y., Ito, T., Kataoka, M., and Tokunaga, F. (1995) Reconstitution photoactive yellow protein from apoprotein and p-coumaric acid derivatives, *FEBS Lett 374*, 157-160.
[68] Mihara, K. i., Hisatomi, O., Imamoto, Y., Kataoka, M., and Tokunaga, F. (1997) Functional Expression and Site-Directed Mutagenesis of Photoactive Yellow Protein, *Journal of Biochemistry 121*, 876-880.
[69] Gottlieb, S. M., Kim, P. W., Rockwell, N. C., Hirose, Y., Ikeuchi, M., Lagarias, J. C., and Larsen, D. S. (2013) Primary Photodynamics of the Green/Red-Absorbing Photoswitching Regulator of the Chromatic Adaptation E Domain from *Fremyella diplosiphon*, *Biochemistry 52*, 8198-8208.
[70] Mix, L. T., Hara, M., Rathod, R., Kumauchi, M., Hoff, W. D., and Larsen, D. S. (2016) Non-Canonical Photocycle Initiation Dynamics of the Photoactive Yellow Protein Domain of the PYP-Phytochrome-Related (Ppr) Photoreceptor *The Journal of Physical Chemistry Letters 7*, 5212-5218.
[71] Yamaguchi, S., Kamikubo, H., Kurihara, K., Kuroki, R., Niimura, N., Shimizu, N., Yamazaki, Y., and Kataoka, M. (2009) Low-barrier hydrogen bond in photoactive yellow protein, *Proceedings of the National Academy of Sciences 106*, 440-444.
[72] Berendsen, H. J. C., Postma, J. P. M., Gunsteren, W. F. v., DiNola, A., and Haak, J. R. (1984) Molecular dynamics with coupling to an external bath, *The Journal of Chemical Physics 81*, 3684-3690.
[73] Bussi, G., Donadio, D., and Parrinello, M. (2007) Canonical sampling through velocity rescaling, *The Journal of Chemical Physics 126*, 014101.
[74] Hess, B., Bekker, H., Berendsen, H. J. C., and Fraaije, J. G. E. M. (1997) LINCS: A linear constraint solver for molecular simulations, *Journal of Computational Chemistry 18*, 1463-1472.
[75] Miyamoto, S., and Kollman, P. A. (1992) Settle: An analytical version of the SHAKE and RATTLE algorithm for rigid water models, *Journal of Computational Chemistry 13*, 952-962.
[76] Essmann, U., Perera, L., Berkowitz, M. L., Darden, T., Lee, H., and Pedersen, L. G. (1995) A smooth particle mesh Ewald method, *The Journal of Chemical Physics 103*, 8577-8593.
[77] van der Spoel, D., Lindahl, E., Hess, B., Groenhof, G., Mark, A. E., and Berendsen, H. J. C. (2005) GROMACS: Fast, flexible, and free, *Journal of Computational Chemistry 26*, 1701-1718.
[78] Duan, Y., Wu, C., Chowdhury, S., Lee, M. C., Xiong, G., Zhang, W., Yang, R., Cieplak, P., Luo, R., Lee, T., Caldwell, J., Wang, J., and Kollman, P. (2003) A point-charge force field for molecular mechanics simulations of proteins based on condensed-phase quantum mechanical calculations, *Journal of Computational Chemistry 24*, 1999-2012.
[79] Schmidt, M. W., Baldridge, K. K., Boatz, J. A., Elbert, S. T., Gordon, M. S., Jensen, J. H., Koseki, S., Matsunaga, N., Nguyen, K. A., Su, S., Windus, T. L., Dupuis, M., and Montgomery, J. A. (1993) General atomic and molecular electronic structure system, *Journal of Computational Chemistry 14*, 1347-1363.
[80] Adamo, C., and Barone, V. (1999) Toward reliable density functional methods without adjustable parameters: The PBE0 model, *The Journal of Chemical Physics 110*, 6158-6170.
[81] Granovsky, A. A. (2011) Extended multi-configuration quasi-degenerate perturbation theory: The new approach to multi-state multi-reference perturbation theory, *The Journal of Chemical Physics 134*, 214113.
[82] Roos, B. O., Taylor, P. R., and Siegbahn, P. E. M. (1980) A complete active space SCF method (CASSCF) using a density matrix formulated super-CI approach, *Chemical Physics 48*, 157-173.
[83] Granovsky, A. A. Firefly Version 8.2.0 Avalible at: http://classic.chem.msu.su/gran/firefly/index.html.
[84] van Stokkum, I. H. M., Larsen, D. S., and van Grondelle, R. (2004) Global and target analysis of time-resolved spectra, *Biochimica et Biophysica Acta (BBA) - Bioenergetics 1657*, 82-104.
[85] Holzwarth, A. (1996) Data Analysis of Time-Resolved Measurements, In *Biophysical Techniques in Photosynthesis* (Amesz, J., and Hoff, A., Eds.), pp 75-92, Springer Netherlands.
[86] Carroll, E. C., Song, S.-H., Kumauchi, M., van Stokkum, I. H. M., Jailaubekov, A., Hoff, W. D., and Larsen, D. S. (2010) Subpicosecond Excited-State Proton Transfer Preceding Isomerization During

the Photorecovery of Photoactive Yellow Protein, *The Journal of Physical Chemistry Letters 1*, 2793-2799.

[87] Changenet-Barret, P., Plaza, P., Martin, M. M., Chosrowjan, H., Taniguchi, S., Mataga, N., Imamoto, Y., and Kataoka, M. (2009) Structural Effects on the Ultrafast Photoisomerization of Photoactive Yellow Protein. Transient Absorption Spectroscopy of Two Point Mutants, *The Journal of Physical Chemistry C 113*, 11605-11613.

[88] Schultz, T., Quenneville, J., Levine, B., Toniolo, A., Martínez, T. J., Lochbrunner, S., Schmitt, M., Shaffer, J. P., Zgierski, M. Z., and Stolow, A. (2003) Mechanism and Dynamics of Azobenzene Photoisomerization, *Journal of the American Chemical Society 125*, 8098-8099.

[89] Rudolf, P., Kanal, F., Knorr, J., Nagel, C., Niesel, J., Brixner, T., Schatzschneider, U., and Nuernberger, P. (2013) Ultrafast Photochemistry of a Manganese-Tricarbonyl CO-Releasing Molecule (CORM) in Aqueous Solution, *The Journal of Physical Chemistry Letters 4*, 596-602.

[90] Gromov, E. V., Burghardt, I., Koppel, H., and Cederbaum, L. S. (2007) Electronic structure of the PYP chromophore in its native protein environment, *Journal of the American Chemical Society 129*, 6798-6806.

[91] Coto, P. B., Marti, S., Oliva, M., Olivucci, M., Merchan, M., and Andres, J. (2008) Origin of the absorption maxima of the photoactive yellow protein resolved via ab initio multiconfigurational methods, *Journal of Physical Chemistry B 112*, 7153-7156.

[92] Ryan, W. L., Gordon, D. J., and Levy, D. H. (2002) Gas-Phase Photochemistry of the Photoactive Yellow Protein Chromophore trans-p-Coumaric Acid, *Journal of the American Chemical Society 124*, 6194-6201.

[93] de Groot, M., and Buma, W. J. (2005) Comment on "Gas-Phase Photochemistry of the Photoactive Yellow Protein Chromophore trans-p-Coumaric Acid", *The Journal of Physical Chemistry A 109*, 6135-6136.

[94] Kovalenko, S. A., and Dobryakov, A. L. (2013) On the excitation wavelength dependence and Arrhenius behavior of stilbene isomerization rates in solution, *Chemical Physics Letters 570*, 56-60.

[95] Kim, J. E., Tauber, M. J., and Mathies, R. A. (2001) Wavelength Dependent Cis-Trans Isomerization in Vision, *Biochemistry 40*, 13774-13778.

[96] Frauenfelder, H., Chen, G., Berendzen, J., Fenimore, P. W., Jansson, H., McMahon, B. H., Stroe, I. R., Swenson, J., and Young, R. D. (2009) A unified model of protein dynamics, *Proceedings of the National Academy of Sciences 106*, 5129-5134.

[97] Bu, Z., and Callaway, D. J. E. (2011) Chapter 5 - Proteins MOVE! Protein dynamics and long-range allostery in cell signaling, In *Advances in Protein Chemistry and Structural Biology* (Rossen, D., Ed.), pp 163-221, Academic Press.

[98] Morozov, D., and Groenhof, G. (2016) Hydrogen Bond Fluctuations Control Photochromism in a Reversibly Photo-Switchable Fluorescent Protein, *Angewandte Chemie International Edition 55*, 576-578.

[99] Groenhof, G., Schäfer, L. V., Boggio-Pasqua, M., Grubmüller, H., and Robb, M. A. (2008) Arginine52 Controls the Photoisomerization Process in Photoactive Yellow Protein, *Journal of the American Chemical Society 130*, 3250-3251.

[100] Ko, C., Virshup, A. M., and Martinez, T. J. (2008) Electrostatic control of photoisomerization in the photoactive yellow protein chromophore: Ab initio multiple spawning dynamics, *Chemical Physics Letters 460*, 272-277.

[101] Fisher, S. Z., Anderson, S., Henning, R., Moffat, K., Langan, P., Thiyagarajan, P., and Schultz, A. J. (2007) Neutron and X-ray structural studies of short hydrogen bonds in photoactive yellow protein (PYP), *Acta crystallographica. Section D, Biological crystallography 63*, 1178-1184.

[102] Yonezawa, K., Shimizu, N., Kurihara, K., Yamazaki, Y., Kamikubo, H., and Kataoka, M. (2017) Neutron crystallography of photoactive yellow protein reveals unusual protonation state of Arg52 in the crystal, *Scientific Reports 7*, 9361.

[103] Yoshimura, Y., Oktaviani, N. A., Yonezawa, K., Kamikubo, H., and Mulder, F. A. A. (2017) Unambiguous Determination of Protein Arginine Ionization States in Solution by NMR Spectroscopy, *Angewandte Chemie International Edition 56*, 239-242.

[104] Graen, T., Inhester, L., Clemens, M., Grubmüller, H., and Groenhof, G. (2016) The Low Barrier Hydrogen Bond in the Photoactive Yellow Protein: A Vacuum Artifact Absent in the Crystal and Solution, *Journal of the American Chemical Society 138*, 16620-16631.

[105] Changenet-Barret, P., Plaza, P., Martin, M. M., Chosrowjan, H., Taniguchi, S., Mataga, N., Imamoto, Y., and Kataoka, M. (2007) Role of arginine 52 on the primary photoinduced events in the PYP photocycle, *Chemical Physics Letters 434*, 320-325.

[106] Chosrowjan, H., Mataga, N., Shibata, Y., Imamoto, Y., and Tokunaga, F. (1998) Environmental effects on the femtosecond-picosecond fluorescence dynamics of photoactive yellow protein: Chromophores in aqueous solutions and in protein nanospaces modified by site-directed mutagenesis, *Journal of Physical Chemistry B 102*, 7695-7698.

[107] Mataga, N., Chosrowjan, H., Shibata, Y., Imamoto, Y., and Tokunaga, F. (2000) Effects of modification of protein nanospace structure and change of temperature on the femtosecond to picosecond fluorescence dynamics of photoactive yellow protein, *Journal of Physical Chemistry B 104*, 5191-5199.

[108] Takeshita, K., Imamoto, Y., Kataoka, M., Mihara, K., Tokunaga, F., and Terazima, M. (2002) Structural change of site-directed mutants of PYP: New dynamics during pR state, *Biophysical Journal 83*, 1567-1577.

[109] Düx, P., Rubinstenn, G., Vuister, G. W., Boelens, R., Mulder, F. A. A., Hård, K., Hoff, W. D., Kroon, A. R., Crielaard, W., Hellingwerf, K. J., and Kaptein, R. (1998) Solution Structure and Backbone Dynamics of the Photoactive Yellow Protein, *Biochemistry 37*, 12689-12699.

[110] Groenhof, G., Lensink, M. F., Berendsen, H. J. C., Snijders, J. G., and Mark, A. E. (2002) Signal transduction in the photoactive yellow protein. I. Photon absorption and the isomerization of the chromophore, *Proteins: Structure, Function, and Bioinformatics 48*, 202-211.

[111] Groenhof, G., Bouxin-Cademartory, M., Hess, B., de Visser, S. P., Berendsen, H. J. C., Olivucci, M., Mark, A. E., and Robb, M. A. (2004) Photoactivation of the Photoactive Yellow Protein: Why Photon Absorption Triggers a Trans-to-Cis Isomerization of the Chromophore in the Protein, *Journal of the American Chemical Society 126*, 4228-4233.

[112] Bernard, C., Houben, K., Derix, N. M., Marks, D., van der Horst, M. A., Hellingwerf, K. J., Boelens, R., Kaptein, R., and van Nuland, N. A. J. (2005) The Solution Structure of a Transient Photoreceptor Intermediate: Δ25 Photoactive Yellow Protein, *Structure 13*, 953-962.

[113] Taenzler, P. J., Sadeghian, K., and Ochsenfeld, C. (2016) A Dynamic Equilibrium of Three Hydrogen-Bond Conformers Explains the NMR Spectrum of the Active Site of Photoactive Yellow Protein, *Journal of Chemical Theory and Computation 12*, 5170-5178.

[114] Hutchison, C. D. M., and van Thor, J. J. (2017) Populations and coherence in femtosecond time resolved X-ray crystallography of the photoactive yellow protein, *International Reviews in Physical Chemistry 36*, 117-143.

[115] Changenet-Barret, P., Plaza, P., Martin, M. M., Chosrowjan, H., Taniguchi, S., Mataga, N., Imamoto, Y., and Kataoka, M. (2007) Role of arginine 52 on the primary photoinduced events in the PYP photocycle, *Chemical Physics Letters 434*, 320-325.

[116] Kasha, M. (1950) Characterization of electronic transitions in complex molecules, *Discussions of the Faraday Society 9*, 14-19.

For Table of Contents Use Only

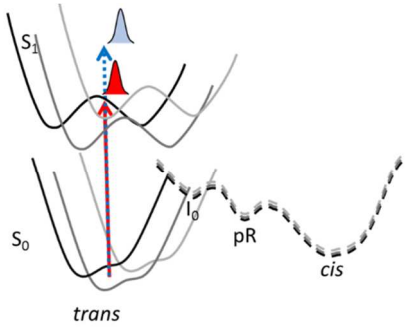

Excitation-Wavelength Dependent Photocycle Initiation Dynamics Resolve Heterogeneity in the Photoactive Yellow Protein from Halorhodospira halophila

L. Tyler Mix[†], Elizabeth C. Carroll[†a], Jie Pan[†b], Dmitry Morozov[ϕ], Wendy Ryan Gordon[#c], Andrew Philip[⊥d], Ivo van Stokkum[‡], Masato Kumauchi[§e], Gerrit Groenhof[ϕ], Wouter D. Hoff*[§], and Delmar S. Larsen[†]